1 **Title:** The fate of carbon in a mature forest under carbon dioxide enrichment

2 M. Jiang[1], B.E. Medlyn[1], J.E. Drake[1,2], R.A. Duursma[1], I.C. Anderson[1], C.V.M. Barton[1],

3 M.M. Boer[1], Y. Carrillo[1], L.Castañeda-Gómez[1], L. Collins[1,3,4], K.Y. Crous[1], M.G. De

4 Kauwe[5,6,7], B.M. dos Santos[8,9], K.M. Emmerson[10], S.L. Facey[1], A.N. Gherlenda[1], T.E.

5 Gimeno[1,11,12], S. Hasegawa[1,13], S.N. Johnson[1], C.A. Macdonald[1], K. Mahmud[1,14], A.

6 Kännaste[15], B.D. Moore[1], L. Nazaries[1], E.H.J. Neilson[8,9], U.N. Nielsen[1], Ü. Niinemets[15], N.J.

7 Noh[1,16], R. Ochoa-Hueso[1,17], V.S. Pathare[1,18], E. Pendall[1], J. Pihlblad[1], J. Pineiro[1,19], J.R.

8 Powell[1], S.A. Power[1], P.B. Reich[1,20], A.A. Renchon[1], M. Riegler[1], R. Rinnan[21], P. Rymer[1],

9 R.L. Salomón[22], B.K. Singh[1,23], B. Smith[1,24], M.G. Tjoelker[1], J.K.M. Walker[1], A. Wujeska-

10 Klause[1], J. Yang[1], S. Zaehle[25], and D.S. Ellsworth[1]

11

12 **Affiliation:**

13 [1]Hawkesbury Institute for the Environment, Western Sydney University, Locked Bag 1797,

14 Penrith, NSW, 2751, Australia

15 [2]Department of Sustainable Resources Management, College of Environmental Science and

16 Forestry, State University of New York, Syracuse, NY 13210, USA

17 [3]Department of Ecology, Environment and Evolution, La Trobe University, Bundoora, VIC

18 3086, Australia

19 [4]Arthur Rylah Institute for Environmental Research, Department of Environment, Land,

20 Water and Planning, PO Box 137, Heidelberg, VIC 3084, Australia

21 [5]ARC Centre of Excellence for Climate Extremes, University of New South Wales, Sydney,

22 NSW 2052, Australia

23 [6]Climate Change Research Centre, University of New South Wales, Sydney, NSW, 2052,

24 Australia

25 [7]Evolution and Ecology Research Centre, University of New South Wales, Sydney, NSW,

26 2052, Australia

27 [8]Plant Biochemistry Laboratory, Department of Plant and Environmental Sciences, University

28 of Copenhagen, Thorvaldsensvej 40, 1871 Frederiksberg C, Copenhagen, Denmark

29 [9]VILLUM Research Center for Plant Plasticity, University of Copenhagen, Thorvaldsensvej

30 40, 1871 Frederiksberg C, Copenhagen, Denmark

31 [10]Climate Science Centre, CSIRO Oceans & Atmosphere, Aspendale, VIC 3195, Australia

32 [11]Basque Centre for Climate Change, Leioa, 48940, Spain

33 [12]Ikerbasque, Basque Foundation for Science, 48008 Bilbao, Spain

34 [13]Department of Forest Ecology and Management, Swedish University of Agricultural

35 Sciences (SLU), Umeå, SE-90183, Sweden

36 [14]Department of Geography, Indiana University, Bloomington, IN 47405, USA

37 [15]Estonian University of Life Sciences, Kreutzwaldi 1, 51006, Tartu, Estonia

38 [16]Forest Technology and Management Research Center, National Institute of Forest Science,

39 Gyeonggi-do, 1186, Korea

40 [17]Department of Biology, IVAGRO, University of Cádiz, Campus de Excelencia

41 Internacional Agroalimentario (CeiA3), Campus del Rio San Pedro, 11510 Puerto Real,

42 Cádiz, Spain

43 [18]School of Biological Sciences, Post Office Box 646340, Washington State University,

44 Pullman, WA 99164-6340, USA

45 [19]Division of Plant and Soil Sciences, West Virginia University, Morgantown, WV, USA

46 [20]Department of Forest Resources, University of Minnesota, St Paul, Minnesota, 55108, USA

47 [21]Terrestrial Ecology Section, Department of Biology, University of Copenhagen,

48 Universitetsparken 15, DK-2100, Copenhagen, Denmark

49 [22]Laboratory of Plant Ecology, Faculty of Bioscience Engineering, Ghent University, Coupure links 653, 9000 Ghent, Belgium

51 [23]Global Centre for Land Based Innovation, Western Sydney University, Building L9, Locked Bag 1797, Penrith South, NSW, 2751, Australia

53 [24]Department of Physical Geography and Ecosystem Science, Lund University, 22362, Lund, Sweden

55 [25]Max Planck Institute for Biogeochemistry, Hans-Knöll-Str. 10, 07745 Jena, Germany

Abstract

Atmospheric carbon dioxide enrichment (eCO$_2$) can enhance plant carbon uptake and growth[1,2,3,4,5], thereby providing an important negative feedback to climate change by slowing the rate of increase of the atmospheric CO$_2$ concentration[6]. While evidence gathered from young aggrading forests has generally indicated a strong CO$_2$ fertilization effect on biomass growth[3,4,5], it is unclear whether mature forests respond to eCO$_2$ in a similar way. In mature trees and forest stands[7,8,9,10], photosynthetic uptake has been found to increase under eCO$_2$ without any apparent accompanying growth response, leaving an open question about the fate of additional carbon fixed under eCO$_2$[4,5,7,8,9,10,11]. Here, using data from the first ecosystem-scale Free-Air CO$_2$ Enrichment (FACE) experiment in a mature forest, we constructed a comprehensive ecosystem carbon budget to track the fate of carbon as the forest responds to four years of eCO$_2$ exposure. We show that, although the eCO$_2$ treatment of ambient +150 ppm (+38%) induced a 12% (+247 g C m^{-2} yr^{-1}) increase in carbon uptake through gross primary production, this additional carbon uptake did not lead to increased carbon sequestration at the ecosystem level. Instead, the majority of the extra carbon was emitted back into the atmosphere via several respiratory fluxes, with increased soil respiration alone accounting for ~50% of the total uptake surplus. Our results call into question the predominant thinking that the capacity of forests to act as carbon sinks will be generally enhanced under eCO$_2$, and challenge the efficacy of climate mitigation strategies that rely on ubiquitous CO$_2$ fertilization as a driver of increased carbon sinks in global forests.

Main text

Globally, forests act as a large carbon sink, absorbing a significant portion of the anthropogenic CO$_2$ emissions[1,12], an ecosystem service that has tremendous social and

80   economic value. Whether mature forests will remain carbon sinks into the future is of critical

81   importance for aspirations to limit climate warming to no more than 1.5 °C above pre-

82   industrial levels[13]. Free-Air CO_2 Enrichment (FACE) experiments provide an opportunity to

83   determine the capacity of ecosystems to sequester carbon under the higher atmospheric CO_2

84   concentrations expected in the future[3,4,5,7,8,10,11]. Evidence gathered from the four first-

85   generation forest FACE experiments, which all measured responses of rapidly-growing

86   young forest plantations, has generally indicated a strong CO_2 fertilization effect on biomass

87   growth[3,4]. This CO_2 fertilization effect has been hypothesized to be one of the largest drivers

88   of the terrestrial carbon sink and its acceleration in recent decades[14], potentially accounting

89   for up to 60% of present-day terrestrial carbon sequestration[2]. However, younger trees are

90   generally more responsive to rising CO_2 than mature trees[11], potentially because nutrient

91   limitation increases with stand age[15]. Thus, extrapolating evidence collected from these

92   experiments may be argued to provide an upper limit on how much carbon can be stored by

93   global forests under eCO_2[16]. Evidence from experiments with older trees on nutrient-poor

94   soils suggests that although eCO_2 increases leaf photosynthesis to a similar degree as in

95   young forests, stimulation of biomass growth and carbon storage may be lower or

96   absent[7,8,9,10]. Reconciling these conflicting observations is a crucial step towards quantifying

97   the carbon sequestration capacity of mature forests in the future. It requires that we identify

98   the fate of the extra carbon fixed under eCO_2 in mature forests, which are expected to be

99   closer to a state of equilibrium between carbon uptake and turnover, compared to young

100   aggrading stands.

101

102   The *Eucalyptus* FACE (EucFACE) experiment is the world's first replicated, ecosystem-scale

103   mature forest FACE experiment (Extended Data Figure 1, 2). It is located in a warm-

104   temperate evergreen forest that has remained undisturbed for the past 90 years, is dominated

105   by the regionally widespread tree *Eucalyptus tereticornis* and has an understorey composed

106   principally of native grasses and shrubs. The low-fertility soil has been shown to limit tree

107   growth in an adjacent phosphorus-fertilization experiment[17]. Seven ecosystem-scale models

108   were used to predict the eCO_2 response at EucFACE in advance of the experiment[18],

109   highlighting three alternative hypotheses for the expected ecosystem response based on

110   plausible assumptions incorporated in different models[19]. These hypotheses were: (i)

111   enhanced photosynthesis under eCO_2 would lead to increased biomass accumulation; (ii)

112   eCO_2-induced increase in photosynthesis would be directly down-regulated by limited

113   nutrient availability; or (iii) eCO_2-induced increase in photosynthesis would lead to increased

114   autotrophic respiration[18]. This range of predictions among a suite of well-tested models

115   indicated a prognostic knowledge gap as to how the carbon cycling of mature forests would

116   respond to the expected rise in atmospheric CO_2 concentration[11], which is crucial to resolve in

117   the face of future carbon-climate uncertainty[20].

118

119   To date, both canopy trees and understorey plants at EucFACE have shown increased rates of

120   leaf photosynthesis but the canopy trees showed no significant increase in aboveground

121   biomass growth under eCO_2[7], reflecting a similar lack of response observed in other eCO_2

122   experiments on mature trees[8,9,10]. Incorporating leaf-scale gas exchange measurements into a

123   process-based tree stand model, it was estimated that the observed +19% stimulation of light-

124   saturated overstorey leaf photosynthesis[7] corresponded to a +11% stimulation of whole-

125   canopy gross primary production (GPP) in response to eCO_2[21]. However, the probable fate of

126   the extra carbon fixed under eCO_2 remained undetermined. Where did the extra carbon go?

127

128   To answer this question, we compiled measurements on all major carbon pools and fluxes

129   collected over four years of experimental treatment (2013-2016), including individual and

130   aggregated biomass and associated fluxes measured or inferred from plants, litter, soil,

131   microbes, and insects, and constructed an ecosystem carbon budget (Figure 1) under both

132   ambient (aCO$_2$) and eCO$_2$ conditions (+150 ppm). We first confirmed mass balance of the

133   ecosystem carbon budget by checking agreement between independent estimates of GPP and

134   soil respiration (R$_{soil}$) derived from separate data streams (Extended Data Figure 3; see

135   Methods). For GPP of the aCO$_2$ plots, we confirmed that a process-based model estimate of

136   overstorey and understorey GPP (2059 ± 211 g C m^{-2} yr^{-1}), driven by site-specific

137   meteorology and treatment-specific physiological data, broadly agreed with the sum of data-

138   driven estimates of net primary production (NPP) and autotrophic respiration (2068 ± 61 g C

139   m^{-2} yr^{-1}). The carbon-use efficiency (NPP/GPP) of this mature forest was estimated to be 0.31

140   ± 0.03, which is on the low end of global forest estimates, but consistent with studies that

141   have observed this ratio to decline with stand age[22] (Extended Data Figure 2). We further

142   confirmed carbon mass balance for R$_{soil}$ of the aCO$_2$ plots by comparing soil chamber-based

143   estimates (1097 ± 86 g C m^{-2} yr^{-1}) with the sum of litterfall and independently estimated root

144   respiration (1086 ± 14 g C m^{-2} yr^{-1}), assuming no change in soil carbon pool (see Methods).

145   This agreement between independent estimates of components of the ecosystem carbon

146   budget gives confidence that our measurements captured the pools and fluxes of carbon with

147   low aggregate uncertainty and hence allow us to infer the fate of the extra carbon fixed under

148   eCO$_2$.

149

150   To accommodate the inherent pre-treatment plot differences (see Methods), we normalized

151   the CO$_2$ responses across plots by using a linear mixed-model with plot-specific pre-

152   treatment leaf area index as a covariate[23,24]. The non-normalized eCO$_2$ responses are provided

153   in Extended Data Figure 4, and generally confirm the findings but with larger uncertainty.

154   Our normalized responses (Figure 2, Extended Data Figure 5) showed that eCO$_2$ induced an

155   average of 12% increase ($+247 \pm 195$ g C m^{-2} yr^{-1}, mean $\pm$ one standard deviation) in carbon

156   uptake, including contributions of overstorey ($+192 \pm 193$ g C m^{-2} yr^{-1}) and understorey GPP

157   ($+55 \pm 21$ g C m^{-2} yr^{-1}). The fate of this additional carbon entering the system under eCO_2

158   was primarily traced to an increase in R_{soil} ($+128.8 \pm 116.7$ g C m^{-2} yr^{-1}, or 52% of the carbon

159   uptake surplus), followed by a smaller increase in tree stem respiration (R_{stem}; $+40.0 \pm 43.6$ g

160   C m^{-2} yr^{-1}, or 16% of the carbon uptake surplus). In comparison, the increase in total NPP

161   ($+67.3 \pm 12.7$ g C m^{-2} yr^{-1}, or 28% of the carbon uptake surplus) corresponded to a smaller

162   increase in storage of the total carbon pools at the ecosystem-level (ΔC_{pools}; $+31.6 \pm 188.8$ g C

163   m^{-2} yr^{-1}, or 12.8% of the carbon uptake surplus, Extended Data Figure 6). There was thus

164   little evidence of additional carbon accumulation under eCO_2 in this mature forest ecosystem.

165   We then compared three alternative methods (see Methods) of estimating net ecosystem

166   production (NEP; Figure 3). All three indicated that the ecosystem remained close to carbon-

167   neutral under ambient CO_2 over the experimental period (mean $\pm$ SD for the methods: $28 \pm$

168   225, 21 ± 129, -73 ± 50 g C m^{-2} yr^{-1}, respectively), and that eCO_2 of +150 ppm did not result

169   in statistically significant increases in ecosystem carbon storage (109 ± 258, -19 ± 171, $-42 \pm$

170   262 g C m^{-2} yr^{-1}, respectively). However, the variability reported here means that we cannot

171   fully rule out the possibility of additional carbon storage under eCO_2, but we stress that our

172   individual and aggregated responses consistently suggest a lack of CO_2 response in this

173   mature forest (Figure 2 & 3, Extended Data Figure 5).

174

175   The relatively small but positive NPP response to eCO_2 was mainly driven by the understorey

176   aboveground NPP response (NPP_{ua}; $+50.3 \pm 17.9$ g C m^{-2} yr^{-1}), which was 75% of the net

177   NPP response (Figure 2). However, this significant NPP_{ua} response did not result in an

178   equivalent eCO_2 effect on understorey aboveground biomass increment ($+27.2 \pm 29.7$ g C m^{-2}

179   yr^{-1}), suggesting a possible higher understorey biomass turnover under eCO_2. Smaller fluxes,

180   often neglected in other ecosystem carbon budgets, such as leaf consumption by insect

181   herbivores (NPP$_{ins}$; 25.5 ± 4.3 vs. 27.8 ± 6.3 g C m^{-2} yr^{-1}, aCO$_2$ vs. eCO$_2$ mean ± SD), insect

182   frass production (Frass; 10.5 ± 1.8 vs. 11.4 ± 2.6 g C m^{-2} yr^{-1}), vegetation volatile carbon

183   emission (VC; 2.63 ± 0.18 vs. 2.45 ± 0.13 g C m^{-2} yr^{-1}), net ecosystem methane uptake (CH$_4$;

184   0.18 ± 0.0009 vs. 0.19 ± 0.0003 g C m^{-2} yr^{-1}), and leaching of dissolved organic carbon (DOC;

185   0.16 ± 0.017 vs. 0.17 ± 0.024 g C m^{-2} yr^{-1}), contributed to the closure of the overall

186   ecosystem carbon budget (Figure 1; Extended Data Figure 3), but were not quantitatively

187   important in explaining pathways of the carbon uptake surplus under eCO$_2$ (Figure 2,

188   Extended Data Figure 5, Extended Data Figure 6).

189

190   Here we provide some of the first replicated experimental evidence on the probable fate of

191   carbon under eCO$_2$ in intact mature forest. We found that increased R$_{soil}$ accounted for ~50%

192   of the extra photosynthate produced by plants under eCO$_2$. It has been suggested that the

193   increase in R$_{soil}$ at EucFACE was likely a consequence of increased root and rhizosphere

194   respiration[25,26], in contrast to other FACE sites where increased R$_{soil}$ was attributed to

195   enhanced soil organic matter decomposition (e.g. DukeFACE[27]). Here, the eCO$_2$-induced

196   increase in R$_{soil}$ was not accompanied by substantial changes in root respiration (18.6 ± 20.1 g

197   C m^{-2} yr^{-1}) or in carbon pools associated with fine roots (+7.0 ± 12.5 g C m^{-2} yr^{-1}), microbes

198   (+1.9 ± 3.5 g C m^{-2} yr^{-1}), mycorrhizae (+0.4 ± 0.5 g C m^{-2} yr^{-1}), leaf litter (+27.1 ± 38.6 g C

199   m^{-2} yr^{-1}) or soil (-23.8 ± 159.6 g C m^{-2} yr^{-1}), suggesting that the additional carbon fixed under

200   eCO$_2$ may have led to an enhanced carbon transport belowground and a rapid belowground

201   turnover of this flux. Assimilation of these data into a carbon balance model supports this

202   inference (Extended Data Figure 7, see Methods for details). An initial enhancement in

203   nitrogen and phosphorus mineralization was observed[28], which suggested that the increased

204   R$_{soil}$ with eCO$_2$ could reflect soil organic matter priming with the potential to alleviate plant

205   nutrient stress in this low-phosphorus soil[28,29]. However, the enhanced soil mineralization rate

206   and associated increase in nutrient availability did not persist over time[28], indicating that this

207   increased belowground carbon allocation and the rapid turnover of this flux was not effective

208   in increasing phosphorus availability to the plants[30].

209

210   The ecosystem carbon budget presented here provides an opportunity to confront the three

211   alternative hypotheses of the response of this system to eCO_2 treatment that emerged from

212   model predictions made in advance of the experiment[18]. Our data do not support any of the

213   three hypotheses. The eCO_2-induced increase in photosynthesis was not strongly down-

214   regulated by low nutrient availability[7,21]; nor did the eCO_2-induced additional carbon uptake

215   lead to additional biomass accumulation, or enhanced aboveground respiration. These

216   predictions reflect common mechanisms by which terrestrial vegetation models implement

217   nutrient limitation of the eCO_2 response[18,19,31,32]. In contrast, our results suggest a direct

218   connection between plant photosynthesis and belowground activity (Extended Data Figure 7),

219   in which increased belowground carbon allocation increased soil respiration at a rate that

220   accounted for half of the extra carbon fixed under eCO_2 (Figure 2). Predictions made in

221   advance of the experiment did not capture this additional belowground carbon flux, despite

222   their general agreement with data on turnover rates of major carbon pools (Extended Data

223   Figure 8). This increased soil respiration has been demonstrated by some models to be an

224   important and often overlooked mechanism that reduces global soil carbon sequestration

225   relative to estimates by many current models[33]. As a consequence of including this rapid

226   turnover of the increased belowground carbon allocation in terrestrial biosphere models, the

227   time-lag in emitting some of the extra carbon via biomass accumulation and litterfall input

228   into the soils may be reduced, thereby leading to faster cycling of carbon[34] and therefore

229   possible different trajectories of carbon-climate predictions for the future.

230

A major form of land-based climate mitigation actions envisaged in the 2015 Paris Agreement is to enhance forest biomass carbon stocks globally through the protection of existing, largely mature, forests, and through afforestation of new areas. The mitigation potential of forests lies in the accumulated stock of ecosystem carbon, not in the short-term rate of forest photosynthesis. The probable fate of additional carbon determined in our study (Figure 2) challenges the current thinking that all non-aggrading mature forests will contribute to enhanced carbon sinks due to CO_2 fertilization[35], which further questions the allowable CO_2 emission targets sourced from existing carbon cycle models[13,36]. Given that the effect of CO_2 fertilization may be one of diminishing returns over time[14], the statistically non-significant eCO_2 effect on NEP (Figure 3), if representative of nutrient-limited mature forest ecosystems generally, suggests an even weaker carbon sink in the future, especially in low-phosphorus systems such as EucFACE. Future research efforts should target a deeper understanding of the nutrient-carbon feedbacks that likely constrain the carbon sink potential of mature forests under eCO_2, and evaluate the implications of a potentially weaker terrestrial land carbon sink in the development of robust mitigation strategies in the face of climate change. More importantly, whilst the terrestrial carbon sink is integral to current strategies for climate change mitigation, our results call for more active reductions of anthropogenic emissions to meet the targets of the Paris Agreement.

249   **Methods**

250   **EucFACE site description**

251   The EucFACE facility (Extended Data Figure 1) is located in a mature evergreen *Eucalyptus*

252   forest on an alluvial spodosol in western Sydney, Australia (33°36'S, 150°44'E). The site has

253   been a remnant patch of native Cumberland Plain woodland since the 1880's and has

254   remained unmanaged for at least the past 90 years, with *Eucalyptus tereticornis* Sm. as the

255   dominant tree species (98% of the overstorey basal area). *Eucalyptus* trees occur naturally

256   across Australia, accounting for 78% of native forest area in Australia[37] and are planted

257   widely around the globe[38]. Infrastructure for six large circular plots (490 m^2 each) was

258   established in 2010. Starting on 18th September 2012, three plots were subjected to free-air

259   CO_2 enrichment treatment using a computer-controlled pre-dilution method. The CO_2

260   concentrations at EucFACE were ramped up over a six-month period, increasing by +30 ppm

261   every five weeks in discrete steps (+30, 60, 90, 120, and 150 ppm). The full elevated CO_2

262   treatment of +150 ppm started on 6th February 2013 during daylight hours over all days of the

263   year. The site is characterized by a humid temperate-subtropical transitional climate with a

264   mean annual temperature of 17.5°C and a mean annual precipitation of 800 mm (Figure S1).

265   The soil is a Holocene alluvial soil of low fertility with low phosphorus content[7,17]. Soil

266   texture is a loamy sand (> 75% sand content) up to 50 cm in depth. From ca. 50 to 300 cm

267   depth, soils are sandy clay loam, with > 30% silt and clay. Average bulk density is 1.39, 1.69

268   and 1.71 g cm^{-3} for depths of 0-10, 10-20 and 20-30 cm, respectively (Figure S2). Permanent

269   groundwater depth is ~11 m below the soil surface[39]. Understorey vegetation is a diverse

270   mixture of 86 species including forbs, graminoids and shrubs[40]. The dominant understorey

271   species is *Microlaena stipoides*, a C_3 perennial grass that accounted for ~70% of herbaceous

272   biomass and responded rapidly to rainfall variability[41].

273

Estimates of carbon pools and fluxes

275 We estimated plot-specific carbon pools and fluxes at EucFACE over 2013-2016 (Extended

276 Data Table 1). We defined pools as a carbon reservoir and annual increments as the annual

277 changes in the size of each reservoir. We compartmentalized the ecosystem into 11 carbon

278 pools, namely overstorey leaf (C_{ol}), stem (C_{stem}), fine root (C_{froot}), coarse root (C_{croot}),

279 intermediate root (C_{iroot}), understorey aboveground (C_{ua}), soil (C_{soil}), microbe (C_{micr}),

280 mycorrhizae (C_{myco}), leaf litter (C_{lit}), and aboveground insect (C_{ins}) carbon pools, and reported

281 pool size in the unit of g C m^{-2}. We defined fluxes as components of the carbon flow through

282 the system, and report them in the unit of g C m^{-2} yr^{-1}. All annual incremental changes in

283 carbon pools were reported in g C m^{-2} yr^{-1} with a symbol Δ. We converted estimates of

284 biomass into carbon content using variable-specific carbon fractions (*f*) defined in Extended

285 Data Table 2. Below we describe how each pool and flux was estimated.

286

287 *Pools*

288 **Soil carbon pool (C_{soil};** Figure S2**)** was estimated based on quarterly sampled soil carbon

289 content (oven-dried at 40 °C for 48 hours) and plot-specific soil bulk density at three depths

290 (0 - 10 cm, 10 - 20 cm, 20 - 30 cm). Out of the 15 dates when samples were taken, soil carbon

291 content below the top 10 cm of soil was measured on three dates. To obtain a more accurate

292 estimate of annual incremental change in soil carbon pool, we therefore reported soil carbon

293 pool for the top 10 cm only. There were no temporal and eCO$_2$ trends in soil carbon content

294 at deeper depths.

295

296 **Overstorey leaf carbon pool (C_{ol};** Figure S3**)** was estimated based on continuous measures

297 of leaf area index (LAI) and specific leaf area (SLA, m^2 leaf area g^{-1} leaf DM), following C_{ol}

298 $= LAI \times SLA \times f_{ol}$, where f_{ol} is a carbon fraction constant for overstorey leaves (Extended

299 Data Table 2). Daily averages of plot-specific LAI were estimated based on the attenuation of

300 diffuse radiation in a homogenous canopy[24]. The number of observations varies between days,

301 depending on the number of 30-minute cloudy periods. SLA was estimated based on time-

302 series measures of leaf mass per area (LMA), and was then linearly interpolated to plot-

303 specific daily values over time.

304

305 **Stem carbon pool (C_{stem};** Figure S4**)** was estimated based on tree-specific height and

306 diameter at breast height (DBH) measurements, and an allometric scaling relationship derived

307 for *E. tereticornis*[7,42]. DBH changes were measured repeatedly at roughly monthly intervals,

308 at 1.3 m height. Bark was periodically removed from under the dendrometer bands - this

309 effect on DBH was considered by calculating biomass once per year using December data

310 only. Stem biomass data were summed for each plot and averaged over the plot area to obtain

311 ground-based estimates, and was then converted into C_{stem} using treatment-specific carbon

312 fraction (Extended Data Table 2).

313

314 **Understorey aboveground carbon pool (C_{ua}**; Figure S5**)** was estimated at 1-3 month

315 intervals between February 2015 and December 2016 using non-destructive measurements of

316 plant height obtained from stereo-photography[43]. In each of the four 2m × 2m understorey

317 monitoring subplots within each plot, stereo photographs were collected using a Bumblebee

318 XB3 stereo camera (Point Grey Research) mounted ~2.4 m above the ground surface and

319 facing vertically downwards towards the center of the subplot. Stereo images were taken at

320 dusk under diffuse light conditions to avoid measurement errors related to shadows from

321   trees and EucFACE infrastructure. On each sampling date, three sets of stereo photographs

322   were taken in each subplot to produce a large number (i.e. 100,000 s) of understorey plant

323   height estimates from which mean plant height (H_{mean}, in m) was calculated for each plot.

324   Understorey aboveground biomass (B_{ua}, in kg m^{-2}) for each plot was predicted from H_{mean}

325   using an empirical model developed for the grassy understorey vegetation at EucFACE (B_{ua} =

326    $1.72 \times H_{mean} - 0.05$)[43]. The four subplot-level estimates were averaged to obtain a plot-level

327   estimate of B_{ua}, and then converted to an estimate of C_{ua} using a carbon fraction constant

328   (Extended Data Table 2).

329

330   **Root carbon pool (C_{root})** consists of fine root (C_{froot}), intermediate root (C_{iroot}), and coarse

331   root (C_{croot}) pools, with C_{froot} defined as roots with diameter of < 2 mm, C_{iroot} defined as roots

332   with diameter of 2 – 3 mm, and the remaining roots defined as C_{croot} (Figure S6). The C_{root}

333   pool includes roots of both overstorey and understorey vegetation. Total root biomass (B_{root})

334   was estimated based on an allometric relationship with stand basal area (derived from DBH)

335   derived for Australian forest species[44], as follows: $\ln(B_{root}) = 0.787 \times \ln (DBH) + 1.218$.

336

337   Standing intermediate root (2-3 mm in diameter) and fine root biomass (< 2 mm in diameter)

338   were sampled in four subplots per plot at two depths (0 – 10 cm and 10 – 30 cm) in year 2017,

339   whereas only fine root biomass at the same depths with the same number of subplots was

340   repeatedly sampled over the period of 2014-2016[29]. We estimated a depth-specific

341   relationship between fine root biomass (< 2 mm in diameter) and total root biomass less than

342   3 mm in diameter based on samples collected in 2017, and calculated the intermediate root

343   biomass for the period of 2014-2016 based on its corresponding fine root biomass. Coarse

344   root biomass was then estimated as the net difference between total allometrically-derived

345   root biomass and that of roots with diameter < 3mm. The fine, intermediate, and coarse root

346   biomass were multiplied by the corresponding carbon fraction constants to obtain C_{froot}, C_{iroot},

347   and C_{croot}, respectively (Extended Data Table 2).

348

349   **Microbial carbon pool (C_{micr})** was estimated based on fumigation extraction and 0.5 M

350   K_2SO_4 extraction as in Ref. 25 using samples taken at 0-10 cm soil depth over the period of

351   2012 - 2015. Total organic carbon was determined on a Shimadzu TOC analyzer (TOC-L

352   TNM-L; Shimadzu, Sydney, Australia), which was then multiplied by soil bulk density over

353   the same soil depth to obtain the C_{micr} (Figure S7a).

354

355   **Mycorrhizal carbon pool (C_{myco})** for the top 10 cm of soil was estimated via measurements

356   of colonization of mycorrhizal in-growth bags, carbon isotopic partitioning, microbial

357   phospholipid fatty acid abundance and C_{micr}. Nine 45 μm nylon mesh bags (4 × 5 cm) filled

358   with sand, which excluded roots but allowed access of fungi[45], were buried in November

359   2014 in each experimental plot and three bags were subsequently collected every four months

360   for one year. Phospholipid-derived fatty acids (PLFA), a proxy for total microbial biomass

361   abundance, were quantified in sand bags and native field soil following the protocol by Ref

362   46. $δ^{13}C$ values of ground subsamples of this sand, native soil carbon, and aboveground plant

363   tissue (leaves of Eucalypts in April 2014) were used to estimate the fraction of the

364   accumulated carbon in sand bags that was derived from plant carbon using isotopic mass

365   balance. Due to the exclusion of roots, plant-derived carbon in bags can be attributed to

366   mycorrhiza. This plant-derived unitless fraction was then multiplied by the total

367   concentration of PLFA in sand bags to obtain the amount of the total PLFA contributed by

368   mycorrhiza (μg PLFA / g sand). To scale this to native soil PLFA concentrations we then

369   calculated the ratio between mycorrhizal PLFA in sand bags to total PLFA in soil

370 (representing the total microbial pool). Subsequently, to estimate C_{myco}, this ratio was

371 multiplied by the C_{micr} in each plot (Figure S7b).

372

373 **Leaflitter carbon pool (C_{lit})** was estimated based on leaf litter decomposition rate and leaf

374 litterfall data collected by litter baskets (Figure S8)[24]. Leaf litter decomposition rates were

375 estimated over 24 months using litter bags. Briefly, 2 g air-dried *Eucalyptus* litter was added

376 to 10×15 cm litter bags with a 2-mm mesh size. Twelve litter bags were randomly allocated

377 to 4 subplots within each treatment plot, and two litter bags were collected at 3, 6, 9, 12, 18

378 and 24 months to calculate mass loss over time (mass loss was averaged across the two

379 replicates from each subplot). A leaflitter exponential decay function was estimated for each

380 plot, based on data collected over this 24-month period. Leaf litterfall was estimated from

381 monthly collections of material from circular fine-mesh traps (each 0.2 m^2) at eight random

382 locations for each plot. We then applied the exponential decay function with litterfall biomass

383 to obtain C_{lit}, assuming a carbon fraction constant (Extended Data Table 2).

384

385 **Insect carbon pool (C_{ins})** was estimated based on two different sampling techniques, with

386 aerial insects partially estimated based on monthly dead insect data collected from circular

387 fine-mesh traps of 0.2 m^2 at eight random locations for each plot[47], and understory insects

388 estimated based on vacuum suction sampling from two locations for each plot[48]. The insect

389 biomass estimated based on these two sampling techniques may be a conservative estimate

390 (the frass produced would suggest presence of a larger insect biomass[49]); nevertheless, they

391 provided a direct estimate based on data collected *in situ*. The vacuum suction method

392 collected invertebrates from understorey vegetation in two 1×1 m subplots using a petrol-

393 powered 'G-Vac' vacuum device run on full-throttle for 20 s, for a total of five sampling

394 campaigns. Trapping locations were randomly chosen and fixed between sampling

395   campaigns. All invertebrates were sorted from debris, dried to constant weight at 60 °C and

396   weighed on a microbalance with a precision of 1 μg. We assumed that vacuum samples as

397   well as fine-mesh trap samples represent point estimates of invertebrate abundance. Then, the

398   total biomass of sampled invertebrates was summed across sampling methods within each

399   plot. A constant carbon fraction based on Ref 50 (Extended Data Table 2) was used to

400   convert biomass into C_{ins} pool (Figure S9).

401   *Ecosystem carbon uptake fluxes*

402   **Overstorey gross primary production (GPP_O)** for each plot was provided by a stand-level

403   model simulation (MAESPA), forced by hourly meteorological data, daily plot-specific leaf

404   area index and leaf-scale treatment-specific photosynthetic parameters measured at the site

405   (Figure S10a)[7,21]. In short, MAESPA was used as a tool to up-scale leaf-level gas exchange

406   measurements to the whole canopy. In MAESPA, each plot consists of individual tree crowns

407   that are located and parameterized with measured coordinates, crown size, and LAI. Each

408   crown is divided into six layers, with leaf area uniformly distributed in each layer. Within

409   each layer, the model simulates twelve grid points. The incident radiation on the sunlit and

410   shaded leaf area at each grid point is calculated considering shading from upper crown and

411   surrounding trees, solar angle (zenith and azimuth), and light source (diffuse or direct).

412   Incident radiation is then used to calculate gas exchange using a Farquhar[51] formulation for

413   photosynthesis and a Medlyn formulation[52] for stomatal conductance. The model was

414   parameterized with treatment-specific leaf gas exchange measurements made *in situ*[7,53]. Leaf

415   respiration and its temperature dependence were also quantified using data collected on site,

416   then up-scaled to the canopy using MAESPA. The performance of the model was evaluated

417   by comparing the simulated transpiration flux to sap flow data[54].

418

419   Similarly, **understorey GPP (GPP$_u$)** (Figure S10b) was simulated using MAESPA with

420   photosynthetic parameters taken for the dominant grass *Microlaena stipoides*[41]. The

421   parameterization of understory vegetation is different from that of the canopy. In each plot,

422   the understory was assumed to form a single crown covering the whole plot (i.e., a circle with

423   12.5 m radius) at a height of 1.5 m. The LAI of the understory was estimated using

424   phenology camera digital photographs taken at four permanent understorey vegetation

425   monitoring subplots in each plot[43]. The average green pixel content was calculated from three

426   photos in each subplot, and assumed to be the same as the fraction of absorbed PAR. We then

427   assumed a light extinction coefficient of 0.5 in Beers' Law and calculated understorey LAI.

428   Before 2014 there were 3 campaigns per year while from 2014 the cameras were automated,

429   and we used the fortnightly averages. Leaf gas exchange parameters were obtained from Ref

430   41 and covered four to six campaigns per year from 2013 to 2016. We estimated a one-time

431   g_1 parameter[52] for all plots and time, and assumed constant carboxylation rate (V_{cmax}) and

432   electron transport rate (J_{max}) values at 25 ºC across plots. Basal leaf respiration rate and the

433   temperature dependence of photosynthesis and respiration were assumed to be the same as

434   those for the canopy. The understory simulation was conducted separately from the canopy,

435   with canopy LAI from Ref 24 included to account for the shading from the canopy, branches

436   and stems on the understory.

437

438   For the **methane net flux (CH$_4$),** air samples were collected following the closed-chamber

439   method (or Non-Flow-Through Non-Steady-State [NFT-NSS] method). Seven replicated

440   chambers were available for each plot. Headspace samples were collected monthly, over a

441   period of one hour and analyzed by gas chromatography. Fluxes were estimated by a mixture

442   of linear and quadratic regressions (depending on goodness-of-fit), assuming a constant air

443   pressure of one atmosphere and correcting the air temperature inside the chambers for each

444 air sample[55]. The CH_4 fluxes are net fluxes, which represent the sum of: 1) CH_4 efflux

445 (emissions from the soil into the atmosphere); 2) CH_4 influx (uptake from the atmosphere

446 into soil). Here, the annual net CH_4 flux was an ecosystem influx and was presented as

447 positive values (Figure S11a).

448

449 *Production fluxes*

450 Plant **net primary production (NPP)** is the sum of overstorey leaf (NPP_{ol}), stem (NPP_{stem}),

451 fine root (NPP_{froot}), intermediate root (NPP_{iroot}), coarse root (NPP_{croot}), other (including twigs,

452 barks, and seeds; NPP_{other}), understorey aboveground (NPP_{ua}), and consumption of overstorey

453 leaf by insect herbivores (NPP_{ins}). NPP_{ol} and NPP_{other} were estimated based on monthly litter

454 data collected from circular fine-mesh traps of 0.2 m^2 at eight random locations for each plot

455 (Figure S12). Litter was sorted into leaf, twigs, bark, and seeds, dried to constant mass at

456 40 °C and weighed. A subsample was reweighed when dried to constant mass at 70 °C and a

457 small moisture correction[7] was applied to the leaf component of the whole dataset. NPP_{ol} was

458 computed as the sum of annual leaf litter, which excluded leaf consumption by insects. For

459 twigs, we assumed strictly annual turnover across the years. NPP_{stem} (Figure S13) and

460 NPP_{croot} (Figure S14) were estimated based on annual incremental change of stem biomass

461 and coarse root biomass, respectively. NPP_{froot} was estimated based on samples collected

462 from in-growth cores at four different locations per plot (Figure S14). NPP_{iroot} was estimated

463 based on a global mean coarse root turnover rate (0.3605 yr^{-1}) for evergreen broadleaf

464 forests[56], and the C_{iroot} pool in our dataset (Figure S14).

465

466 NPP_{ua} was estimated based on biomass clippings taken between 2015 - 2017, assuming one

467 understorey turnover per harvest interval (Figure S15). We used a clip-strip method of

468 biomass harvest as has been applied previously at the BioCON experiment[57]. Specifically,

469   four narrow strips, each with a size of 1 m × 0.1 m, were situated in each of the experimental

470   plots at least 2 m away from the vertical pipes for FACE, while avoiding the understory

471   shrubs. The understory herbaceous species were clipped approximately 1 cm above soil level.

472   The total mass per harvest represents the total production. Biomass samples were oven dried

473   for two days at 60 $^{\circ}$C, and converted into carbon mass by applying a constant fraction

474   (Extended Data Table 2).

475

476   NPP lost to overstorey leaf consumption by insect herbivores (NPP_{ins}) was estimated based

477   on insect frass data (Frass) collected from the circular fine-mesh traps, and a relationship

478   between frass mass and insect-consumed leaf mass derived based on multiple *Eucalyptus* tree

479   species at different CO_2 concentrations (Figure S16a)[58,59]. Frass was estimated based on

480   annual collection of frass biomass collected from the circular fine-mesh litter traps with their

481   associated carbon content (Extended Data Table 2; Figure S16c).

482

483   *Outfluxes*

484   Leaching lost as **dissolved organic carbon (DOC)** from soils was estimated based on

485   concentrations of DOC in soil solutions, provided by water suction lysimeter measurements[28].

486   Lysimeters were installed to two depths (0 - 15 cm and 35 - 75 cm, which is immediately

487   above the impermeable layer). Here we assumed that DOC reaching deeper depth is lost from

488   the system at a rate of 20 ml m^{-2} d^{-1}, which is an estimate of the daily drainage rate at the site

489   (Figure S11b).

490

491   **Plant autotrophic respiration (R_a)** consists of overstorey leaf (R_{ol}), stem (R_{stem}), root (R_{root}),

492   understorey aboveground (R_{ua}) (Figure S17), and growth respiration (R_{grow}) (Figure S18). R_{ol}

493   and R_{ua} were based on MAESPA simulation (Figure S17a, c), as described in the respective

494   GPP sections. R_{grow} was estimated by taking a constant fraction of 30% of total NPP as

495   measured directly on *E. tereticornis* trees[60].

496

497   R_{stem} was estimated from measurements of stem CO_2 efflux performed in three dominant

498   trees per plot (Figure S17b). Collars were horizontally attached to the stem at an approximate

499   height of 0.75 m, and R_{stem} (nmol CO_2 m^{-2} s^{-1}) was measured with a portable infrared gas

500   analyzer coupled to a soil respiration chamber adapted for this purpose[61]. Measurement

501   campaigns were performed every one or two months from December 2017 to October 2018,

502   and the relationship between R_{stem} and air temperature (T_{air}) was used to extrapolate R_{stem}

503   across the surveyed period, following $R_{stem} = 0.1866 \times 2.84^{T_{air}/10}$ ($r^2 = 0.42$, $p < 0.0001$). R_{stem}

504   was then upscaled to the stand level considering the ratio of stem axial surface per unit of soil

505   surface measured per plot. Stem surface area was inferred from the measured tree diameter

506   based on dendrometer, and a relationship between diameter and stem surface area estimated

507   from the Terrestrial Laser Scanning (TLS) data. Stem surface area and diameter in the TLS

508   data was estimated through quantitative structure models presented in Ref. 62 and 63. TLS

509   data were acquired with a RIEGL VC-400 terrestrial laser scanner (RIEGL Laser

510   Measurement Systems GmbH). Stem surface area was derived from the TLS data following a

511   two-step approach: (i) manually extracting single trees from the registered TLS point cloud;

512   and (ii) deriving parameters for an extracted single tree. Once a tree is extracted from the

513   point cloud, the next step was to strip off the leaves, and segment the point cloud into stem

514   and branches. Finally, the surface of the segments was reconstructed with geometric

515   primitives (cylinders). The method used a cover set approach, where the point cloud was

516   partitioned into small subsets, which correspond to small connected patches in the tree

517   surface.

518

519   R_{root} was partitioned into fine root (R_{froot}), intermediate root (R_{iroot}), and coarse root (R_{croot})

520   respiration (Figure S17d). Mass-based rates of fine root and intermediate root respiration

521   (nmol CO_2 DM g^{-1} s^{-1}) were measured for detached roots sampled by soil cores at 10 cm soil

522   depth at four subplots per plot with a portable infrared gas analyzer coupled to a small root

523   chamber. Measurement campaigns were performed every one or two months from November

524   2018 to July 2019. The relationship between root respiration and soil temperature (T_{soil}) at 10

525   cm soil depth was used to extrapolate the corresponding root respiration rates across the

526   surveyed period, following the equations: $R_{froot} = 1.138 \times 1.614^{0.0479 \times Tsoil}$ ($r^2 = 0.36$, p <

527   0.0001, RMSE = 1.054), and $R_{iroot} = 0.9764 \times 1.586^{0.0641 \times Tsoil}$ ($r^2 = 0.52$, p < 0.0001, RMSE =

528   0.597). The mass-based rate of coarse root respiration was assumed to be the same as the

529   mass-based rate of stem respiration. R_{froot}, R_{iroot} and R_{croot} were then upscaled to the stand

530   level to obtain R_{root} with fine root, intermediate root, and coarse root biomass, respectively.

531

532   **Carbon efflux due to insect respiration (R_{ins})** was estimated as the net difference between

533   NPP_{ins} and Frass, assuming no net change in insect biomass (Figure S16b).

534

535   **Soil respiration (R_{soil}):** The rate of soil CO_2 efflux was measured at eight locations within

536   each plot, where a permanent PVC collar inserted into the soil was co-located with soil TDR

537   probes for continuous measurements of soil temperature (5-cm-depth) and volumetric water

538   content (0 to 21-cm-depth; CS650-L; Campbell Scientific, Logan, UT, USA). R_{soil} was

539   measured manually at all collar locations every 2-3 weeks, in addition to 30-minute

540   measurements using automated chambers (Li-8100-103; Licor) at one location within each

541   plot, resulting in >300,000 observations over the study period[26]. These data were used to

542   parameterize a semi-mechanistic model of R_{soil}, in which R_{soil} was predicted based on

543 measurements of soil properties, soil physics, and measured soil temperature and volumetric

544 water content[64]. This model successfully recreated the observed fluxes (r^2 between predicted

545 and observed survey R_{soil} was 0.65)[26]. Annual sums of R_{soil} were derived by summing the

546 averaged daily fluxes over eight locations within each plot, where daily fluxes at each

547 location were predicted based on the semi-mechanistic model and daily soil temperature and

548 volumetric water content data taken adjacent to each measurement collar. Soil heterotrophic

549 respiration (R_{hetero}) was taken as the net difference between R_{soil} and R_{root} (Figure S19). Total

550 ecosystem respiration (R) was calculated as the sum of R_a, R_{hetero}, R_{ins}, and VC.

551

552 **Volatile carbon (VC;** Figure S20**)** flux as isoprene (C_5H_8) and monoterpenes was estimated

553 using the Model of Emissions of Gases and Aerosols from Nature (MEGAN)[65]. Isoprene

554 represents over half of all volatile organic carbon species emitted by vegetation globally, and

555 is the dominant source of VC emission at our site. A MEGAN box-model was built from the

556 version used in Ref. 66, centered on the EucFACE facility to calculate hourly emissions of

557 isoprene across the period 2013-2016 for all six plots:

558 $$VC = EF \times LAI \times \gamma$$

559 Where EF is the compound-specific basal emission factor, γ is the emission activity factor,

560 accounting for changes in the emission response due to light, temperature, leaf age and soil

561 moisture. The MEGAN simulations were driven by daily input data of LAI, soil moisture,

562 and hourly input data of photosynthetic active radiation, temperature, atmospheric pressure,

563 wind speed and relative humidity.

564

565 The isoprene EFs for ambient and elevated CO_2 plots were derived from in-line

566 photosynthetic gas-exchange measurements coupled with simultaneous volatile isoprenoid

567 sampling. The isoprene was collected onto sterile stainless steel thermal desorption tubes at

568 the same time as gas exchange was measured, and these were capped and later thermally

569 desorbed for off-line volatile analysis in the laboratory using a Shimadzu 2010 Plus GC-MS

570 system connected to a Shimadzu TD20 automated cartridge desorber. The sampling and GC-

571 MS analysis methodology is described in detail in Ref 67. The chromatographic peaks were

572 identified by comparing them to an isoprene standard and reference mass spectra in the NIST

573 Mass Spectral Library (https://www.nist.gov/srd). Monoterpene emissions were sampled

574 during February 2018 using a push-pull headspace technique[68] from enclosed branches

575 containing approximately 10 leaves and trapped on adsorbent cartridges (150 mg Tenax TA

576 and 200 mg Carbograph 1TD, Markets International Limited, United Kingdom) at an outflow

577 rate of 200 ml min^{-1} for 15 min. Before each measurement, the sampling system was

578 equilibrated for 15 min at an inflow rate of 1000 mol min^{-1}. Monoterpenes were analyzed by

579 gas chromatography-mass spectrometry (R7890A Series GC coupled with a 5975C inert

580 MSD/DS Performance Turbo EI System, Agilent Technologies, Inc., Santa Clara, CA, USA),

581 as described by Ref 69. The obtained chromatograms were deconvoluted, analyzed and data

582 retrieved using the software PARADISe[70] version 3.88. Identification of compounds was

583 performed using analytical standards and according to their mass spectra in the NIST11

584 library. Pure analytical standards were used for quantification. The box-model produced

585 isoprene and monoterpenes were converted to carbon content using the respective molecular

586 mass ratios.

587

588 *Net Ecosystem Production*

589 Net ecosystem production (NEP) was estimated based on three different methods that

590 estimated NEP in relatively independent ways (Figure 3), similar to Ref 71. The first method

591 considered NEP as the difference between total ecosystem influx and total ecosystem outflux

592 (i.e. In - Out), which relied on both process-based modeling and empirical upscaling of

593   respiratory fluxes collected from the field. The second method considered NEP as NPP minus

594   R_{hetero} (i.e. NPP - R_{hetero}), with NPP relying mostly on litter-based production estimates, and

595   R_{hetero} relying on R_{soil} and R_{root} estimates. The third method considers NEP as the sum of

596   changes in carbon pools over time in the ecosystem (i.e. ΔC_{pools}), which was mostly

597   determined by biomass estimates. Equations for each method are provided below:

Method	NEP =
In - Out	$GPP_o + GPP_u + CH_4 - R_{ol} - R_{stem} - R_{soil} - R_{ua} - R_{ins} - DOC - VC - R_{grow}$
NPP - R_{hetero}	$NPP_{ol} + NPP_{stem} + NPP_{froot} + NPP_{iroot} + NPP_{croot} + NPP_{other} + NPP_{ua} + NPP_{ins} -$ R_{hetero}
ΔC_{pools}	$\Delta C_{soil}+\Delta C_{ol}+\Delta C_{stem}+\Delta C_{croot}+\Delta C_{froot}+\Delta C_{iroot}+\Delta C_{ua}+\Delta C_{lit}+\Delta C_{ins}+\Delta C_{micr}+\Delta C_{myco}$

598

Carbon budget evaluation

600   We evaluated the mass balance of our estimated ecosystem carbon budget in two ways.

601   Firstly, we compared model simulated GPP with the aggregated sum of NPP and R_a

602   (Extended Data Figure 3a, b). GPP was simulated by a stand-level ecophysiological model,

603   driven by hourly meteorological data and parameterized with site-specific ecological data[20].

604   This GPP should equal to the aggregation of NPP ($NPP_{ol} + NPP_{stem} + NPP_{froot} + NPP_{iroot} +$

605   $NPP_{croot} + NPP_{other} + NPP_{ua} + NPP_{ins}$) and R_a fluxes ($R_{ol} + R_{stem} + R_{root} + R_{ua} + R_{grow}$), which

606   were mostly extrapolated based on field data. Secondly, R_{soil} estimated based on soil collar

607   flux measurements[24] was evaluated against the sum of litterfall and R_{root} (Extended Data

608   Figure 3c, d), assuming minimal changes in soil carbon stock (as change over this short

609   period of time is beyond the detection limit in a complex and slow-growing mature forest

610   ecosystem like EucFACE). Here, litterfall was the sum of $NPP_{ol} + NPP_{froot} + NPP_{iroot} +$

611   NPP$_{other}$ + NPP$_{ua}$ + Frass, and R$_{root}$ was extrapolated based on root biomass and temperature

612   functions.

613

614   **Statistical analyses**

615   We performed linear mixed-model analysis using the "lmer" function within the "lme4"

616   package[72] in software R[73] to determine the CO_2 treatment effect on all reported variables. All

617   fluxes were reported at an annual rate (g C m^{-2} yr^{-1}). In our model, date and CO_2 treatment

618   were considered as fixed factors, plot as a random factor, and plot-specific pre-treatment LAI

619   (i.e. 4-month average LAI before full CO_2 treatment was switched on) as a covariate to

620   account for pre-treatment differences among treatment plots. Normalizing all response

621   variables with a covariate that integrates light, water and nutrient constraints helps to isolate

622   the CO_2 effect[23], as has been done previously at the site[24] and elsewhere[8,23]. Confidence

623   intervals for the CO_2 effect size of individual variables were reported using the function

624   "confint", which applies quantile functions for the t-distribution after model fitting.

625   Confidence intervals for the predicted flux and pool were reported as the standard deviation

626   of the plot-specific totals (n = 3). Similarly, confidence intervals for the aggregated fluxes

627   (e.g. NPP) were reported by summing individual component fluxes that constitutes the

628   aggregated flux for each plot and computing the standard deviations across plots (n = 3).

629   Finally, confidence intervals for the CO_2 effect size (SD$_{agg}$) of some aggregated fluxes (e.g.

630   NPP) were calculated by pooling the standard deviations of the aggregated fluxes for ambient

631   (SD$_{amb}$) and elevated CO_2 treatment (SD$_{ele}$), following:

$$SD_{agg} = \sqrt{\frac{SD_{amb}^2 + SD_{ele}^2}{2}}$$

632

Uncertainty analysis

We applied a Markov Chain Monte Carlo (MCMC) data assimilation algorithm to a simplified carbon cycle framework to make inference of the uncertainties around the fate of carbon in our carbon budget. We simplified our carbon budget into eight pools (Extended Data Figure 7), namely, leaf (C'_{leaf}, which includes overstorey and understorey), wood (C'_{wood}, which includes stem and coarse root), root (C'_{root}, which includes fine root and intermediate root), aboveground litter (C'_{aglit}), belowground litter (C'_{bglit}), mycorrhizae (C'_{myco}), microbe (C'_{micr}), and soil (C'_{soil}). Here, C'_{aglit} and C'_{bglit} were assumed unknowns and inferred from the analysis. Net primary production (NPP) was calculated as the difference of gross primary production (GPP) and autotrophic respiration (R_a). NPP was then allocated into the four plant carbon pools (C'_{leaf}, C'_{wood}, C'_{root}, and C'_{myco}), with the respective fitted allocation coefficients (a_{leaf}, a_{wood}, a_{root}, and a_{myco}) being inferred. It has been shown that plant carbon allocation to mycorrhizal fungi may be an important flux in forest carbon budget calculation[74]. Turnover rates of C'_{leaf}, C'_{root}, C'_{myco}, C'_{aglit}, C'_{bglit}, C'_{micr} and C'_{soil} were represented by the corresponding turnover coefficients (τ_{leaf}, τ_{wood}, τ_{root}, τ_{myco}, τ_{aglit}, τ_{bglit}, τ_{micr}, τ_{soil}), all of which were assumed unknowns except τ_{wood} (estimated based on litter basket data of twigs, barks and seeds) and τ_{aglit} (estimated from the leaf litter decomposition data). For carbon leaving from C'_{aglit}, C'_{bglit} and C'_{micr}, we inferred the corresponding fractional coefficient that determines the fraction of carbon entering into the next pool (f'_{aglit}, f'_{bglit}, and f'_{micr}), and assumed the remainder to be respired as part of R_{hetero}. The turnover of soil carbon (i.e. τ_{soil}) also contributed to R_{hetero}. In total, we fitted 2 pools, 4 allocation coefficients, 6 turnover rates, and 3 fractional coefficients using the MCMC algorithm.

We used plot-level estimates of GPP, R_a, R_{hetero}, carbon pools and changes in pools to constrain the MCMC fitting. We assumed uniform parameter distributions and a burn-in

658 coefficient of 10%. Chain lengths were set at 200,000 for the ambient CO_2 plots and 500,000

659 for the elevated plots. The longer chain length for the elevated plots was due to the smaller

660 proposal step size for these plots to meet an acceptance rate of around 20%. We reported the

661 means and standard deviation of the estimated parameters at the treatment level in Extended

662 Data Figure 7.

663

664 **Data statement**

665 Data will be available via Figshare (DOI: 10.6084/m9.figshare.11634315) with the

666 publication of the manuscript. Code to process the data is available via GitHub

667 (https://github.com/mingkaijiang/EucFACE_Carbon_Budget/releases/tag/V20200120).

References for main text

1. Le Quéré, C.L. *et al.* Global carbon budget 2018. *Earth Syst. Sci. Data* **10**, 2141-2194 (2018).

2. Schimel, D., Stephens, B.B., and Fisher, J.B. Effect of increasing CO_2 on the terrestrial carbon cycle. *Proc. Natl. Acad. Sci. USA* **112**, 436-441 (2015).

3. Walker, A.P. *et al.* Decadal biomass increment in early secondary successional woody ecosystems is increased by CO_2 enrichment. *Nat. Commun.* **10**, 454, https://doi.org/10.1038/s41467-019-08348-1 (2019).

4. Norby, R.J. and Zak, D.R. Ecological lessons from Free-Air CO_2 Enrichment (FACE) experiments. *Annu. Rev. Ecol. Evol. Syst.* **42**, 181-203 (2011).

5. Leuzinger, S. and Hattenschwiler, S. Beyond global change: lessons from 25 years of CO_2 research. *Oecologia* **171**, 639-651 (2013).

6. Arora, V.K. *et al.* Carbon-concentration and carbon-climate feedbacks in CMIP5 Earth system models. *J. Clim.* **26**, 5289-5214 (2013).

7. Ellsworth, D.S. *et al.* Elevated CO_2 does not increase eucalypt forest productivity on a low-phosphorus soil. *Nat. Clim. Change* **7**, 279-282 (2017).

8. Körner, C. *et al.* Carbon flux and growth in mature deciduous forest trees exposed to elevated CO_2. *Science* **309**, 1360-1362 (2005).

9. Ryan, M.G. Three decades of research at Flakaliden advancing whole-tree physiology, forest ecosystem and global change research. *Tree Physiol.* **33**, 1123-1131 (2013).

10. Klein, T. *et al.* Growth and carbon relations of mature *Picea abies* trees under 5 years of free-air CO_2 enrichment. *J. Ecol.* **104**, 1720-1733 (2016).

11. Norby, R.J. *et al.* Model-data synthesis for the next generation of forest free-air CO_2 enrichment (FACE) experiments. *New Phytol.* **209**, 17-28 (2016).

12. Pugh, T.A.M. *et al.* Role of forest regrowth in global carbon sink dynamics. *Proc. Natl. Acad. Sci. USA* **116**, 4382-4387 (2019).

13. Grassi, G. *et al.* The key role of forests in meeting climate targets requires science for credible mitigation. *Nat. Clim. Change* **7**, 220-226 (2017).

14. Peñuelas, J. *et al.* Shifting from a fertilization-dominated to a warming-dominated period. *Nat. Ecol. Evol.* **1**, 1438-1445 (2017).

15. Luo, Y. *et al.* Progressive nitrogen limitation of ecosystem response to rising atmospheric carbon dioxide. *BioScience* **54**, 731-739.

16. DeLucia, E.H. *et al.* Net primary production of a forest ecosystem with experimental CO_2 enrichment. *Science* **285**, 1177-1179 (1999).

17. Crous, K., Ósvaldsson, A., and Ellsworth, D.S. Is phosphorus limiting in a mature *Eucalyptus* woodland? Phosphorus fertilization stimulates stem growth. *Plant Soil* **391**, 293-305 (2015).

18. Medlyn, B.E. *et al.* Using models to guide field experiments: a priori predictions for the CO_2 response of a nutrient- and water-limited native Eucalypt woodland. *Global Change Biol.* **22**, 2834-2851 (2016).

19. Medlyn, B.E. *et al.* Using ecosystem experiments to improve vegetation models. *Nat. Clim. Change* **5**, 528-534 (2015).

20. Friedlingstein, P. *et al*. Uncertainties in CMIP5 climate projections due to carbon cycle feedbacks. *J. Clim.* **27**, 511-526 (2014).

21. Yang, J. *et al.* Low sensitivity of gross primary production to elevated CO_2 in a mature Eucalypt woodland. *Biogeosciences*. DOI: https://doi.org/10.5194/bg-2019-272 (2020).

22. De Lucia, E.H., Drake, J.E., Thomas, R.B., and Gonzalez-Meler, M. Forest carbon use efficiency: is respiration a constant fraction of gross primary production? *Global Change Biol.* **13**, 1157-1167 (2007).

23. Norby, R.J. Forest canopy productivity index. *Nature* **381**, 564 (1996).

24. Duursma, R.A. *et al*. Canopy leaf area of a mature evergreen Eucalyptus woodland does not respond to elevated atmospheric CO_2 but tracks water availability. *Global Change Biol.* **22**, 1666-1676 (2016).

25. Drake, J.E. *et al.* Short-term carbon cycling responses of a mature eucalypt woodland to gradual stepwise enrichment of atmospheric CO_2 concentration. *Global Change Biol.* **22**, 380-390 (2016).

26. Drake, J.E. *et al.* Three years of soil respiration in a mature eucalypt woodland exposed to atmospheric CO_2 enrichment. *Biogeochemistry* **139**, 85-101 (2018).

27. Drake, J.E. *et al.* Increases in the flux of carbon belowground stimulate nitrogen uptake and sustain the long-term enhancement of forest productivity under elevated CO_2. *Ecol. Lett*. **14**, 349-357 (2011).

28. Hasegawa, S., Macdonald, C.A., and Power, S.A. Elevated carbon dioxide increases soil nitrogen and phosphorus availability in a phosphorus-limited *Eucalyptus* woodland. *Global Change Biol.* **22**, 1628-1643 (2016).

29. Ochoa-Hueso, R. *et al.* Rhizosphere-driven increase in nitrogen and phosphorus availability under elevated atmospheric CO_2 in a mature *Eucalyptus* woodland. *Plant Soil* **416**, 283-295 (2017).

30. Crous, K.Y., Wujeska-Klause, A., Jiang, M., Medlyn, B.E. and Ellsworth, D.S. Nitrogen and phosphorus retranslocation of leaves and stemwood in a mature *Eucalyptus* forest exposed to 5 years of elevated CO_2. *Front. Plant Sci.* **10**:664, doi: 10.3389/fpls.2019.00664 (2019).

740 31. Zaehle, S. *et al*. Evaluation of 11 terrestrial carbon-nitrogen cycle models against

741   observations from two temperature Free-Air CO_2 Enrichment studies. *New Phytol.*

742   **202**, 803-822 (2014).

743 32. Fleischer, K. *et al*. Amazon forest response to CO_2 fertilization dependent on plant

744   phosphorus acquisition. *Nat. Geosci.* **12**, 736-741 (2019).

745 33. Todd-Brown, K.E.O. *et al*. Changes in soil organic carbon storage predicted by earth

746   system models during the 21st century. *Biogeosciences*, **11**, 2341-2356 (2014).

747 34. Kuzyakov, Y., Horwath, W.R., Dorodnikov, M. and Blagodatskaya, E. Review and

748   synthesis of the effects of elevated atmospheric CO_2 on soil processes: no changes in

749   pools, but increased fluxes and accelerated cycles. *Soil Biol. Biochem*. **128**, 66-78

750   (2019).

751 35. Luyssaert, S. *et al*. Old-growth forests as global carbon sinks. *Nature* **455**, 213-215

752   (2008).

753 36. Jones, C. *et al*. 21st century compatible CO_2 emissions and airborne fraction

754   simulated by CMIP5 Earth System models under 4 representative concentration

755   pathways. *J. Clim*. **26**, doi:10.1175–JCLI–D–12–00554.1 (2013).

756

757

758 **Reference for Methods**

759 37. Australia Government Department of Agriculture, Fisheries and Forestry. Australia's

760   agriculture, fisheries and forestry at a glance 2012. Canberra, Australia (2012).

761 38. Food and Agricultural Organization of the United Nations. Global Forest Resources

762   Assessment 2000. FAO Forestry Paper 140. Rome, Italy (2001).

763   39. Gimeno, T.E., McVicar, T.R., O'Grady, A.P., Tissue, D.T. and Ellsworth, D.S. Elevated CO_2 did not affect the hydrological balance of a mature native *Eucalyptus* woodland. *Global Change Biol.* **24**, 3010-3024 (2018).

766   40. Hasegawa, S. *et al*. Elevated CO_2 concentrations reduce C_4 cover and decrease diversity of understorey plant community in a *Eucalyptus* woodland. *J. Ecol.* **106**, 1483–1494 (2018).

769   41. Pathare, V.S. *et al*. Water availability affects seasonal CO_2-induced photosynthetic enhancement in herbaceous species in a periodically dry woodland. *Global Change Biol.* **23**, 5164–5178 (2017).

772   42. Paul, K.I. *et al.* Development and testing of allometric equations for estimating above-ground biomass of mixed-species environmental plantings. *For. Ecol. Manage.* **310**, 483-494 (2013).

775   43. Collins, L. *et al.* Understorey productivity in temperate grassy woodland responds to soil water availability but not to elevated CO_2. *Global Change Biol.* **24**, 2366-2376 (2018).

778   44. Snowdon, P. *et al.* National carbon accounting system technical report no. 17. Australian Greenhouse Office, Canberra, Australia (2000).

780   45. Wallander, H. *et al.* Evaluation of methods to estimate production, biomass and turnover of ectomycorrhizal mycelium in forests soils – A review. *Soil Biol. Biochem.* **57**, 1034–1047 (2013).

783   46. Buyer, J.S. and Sasser, M. High throughput phospholipid fatty acid analysis of soils. *Appl. Soil Ecol*. **61**, 127–130 (2012).

785   47. Gherlenda, A.N., Esveld, J.L., Hall, A.A.G., Duursma, R.A. and Riegler, M. Boom and bust: rapid feedback responses between insect outbreak dynamics and canopy leaf area impacted by rainfall and CO_2. *Global Change Biol*. **22**, 3632-3641 (2016).

788   48. Facey, S.L. *et al*. Atmospheric change causes declines in woodland arthropods and
789   impacts specific trophic groups. *Agr. Forest Entomol.* **19**, 101-112 (2017).

790   49. Murray, T.J.*,* Tissue, D.T., Ellsworth, D.S. and Riegler, M. Interactive effects of pre-
791   industrial, current and future CO_2 and temperature on an insect herbivore of
792   *Eucalyptus*. *Oecologia* **171**, 1025-1035 (2013).

793   50. Trakimas, G. *et al*. Ecological Stoichiometry: a link between developmental speed
794   and physiological stress in an omnivorous insect. *Front. Behav. Neurosci*.
795   **13**:42, https://doi.org/10.3389/fnbeh.2019.00042 (2019).

796   51. Farquhar, G.D. von Caemmerer, S. and Berry, J.A. A biochemical model of
797   photosynthetic CO_2 assimilation in leaves of C3 species. *Planta* **149**, 78–90 (1980).

798   52. Medlyn, B.E. *et al.* Reconciling the optimal and empirical approaches to modelling
799   stomatal conductance. *Global Change Biol*. **17**, 2134–2144 (2011).

800   53. Gimeno, T.E. *et al*. Conserved stomatal behavior under elevated CO_2 and varying
801   water availability in a mature woodland. *Funct. Ecol*. **30**, 700-709 (2016).

802   54. Yang, J. *et al.* Incorporating non-stomatal limitation improves the performance of leaf
803   and canopy models at high vapor pressure deficit. *Tree Physiol*. DOI:
804   https://doi.org/10.1093/treephys/tpz103 (2019).

805   55. Martins, C.S.C. *et al.* Identifying environmental drivers of greenhouse gas emissions
806   under warming and reduced rainfall in boreal-temperate forests. *Funct. Ecol*. **31**,
807   2356–2368 (2017).

808   56. Zhang, X. and Wang, W. The decomposition of fine and coarse roots: their global
809   patterns and controlling factors. *Sci. Rep.* **5**:09940 (2015).

810   57. Reich, P.B. *et al.* Plant diversity enhances ecosystem responses to elevated CO_2 and
811   nitrogen deposition. *Nature* **410**, 809-810 (2001).

812   58. Gherlenda, A.N.*,* Moore, B.D., Haigh, A.M., Johnson, S.N. and Riegler, M. Insect

813   herbivory in a mature *Eucalyptus* woodland canopy depends on leaf phenology but

814   not CO_2 enrichment. *BMC Ecol.* **16**, 47 (2016).

815   59. Gherlenda, A.N. *et al*. Precipitation, not CO_2 enrichment, drives insect herbivore frass

816   deposition and subsequent nutrient dynamics in a mature *Eucalyptus* woodland. *Plant*

817   *Soil* **399**, 29-39 (2016).

818   60. Drake, J.E. *et al*. The partitioning of gross primary production for young *Eucalyptus*

819   *tereticornis* trees under experimental warming and altered water availability. *New*

820   *Phytol*. **222**, 1298-1312 (2019).

821   61. Salomón, R.L., Steppe, K., Crous, K.Y., Noh, N.J. and Ellsworth, D.S. Elevated CO_2

822   does not affect stem CO_2 efflux nor stem respiration in dry *Eucalyptus* woodland, but

823   it shifts the vertical gradient in xylem CO_2. *Plant Cell Environ.* **42**, 2151-2164 (2019).

824   62. Raumonen, P. *et al*. Fast Automatic Precision Tree Models from Terrestrial Laser

825   Scanner Data. *Remote Sens.* **5**, 491-520 (2013).

826   63. Calders, K. *et al.* Nondestructive estimates of above-ground biomass using terrestrial

827   laser scanning. *Methods Ecol. Evol.* **6**, 198-208 (2015).

828   64. Davidson, E.A., Samanta, S., Caramori, S.S. and Savage, K. The Dual Arrhenius and

829   Michaelis–Menten kinetics model for decomposition of soil organic matter at hourly

830   to seasonal time scales. *Global Change Biol.* **18**, 371-384 (2012).

831   65. Guenther, A.B. *et al.* The Model of Emissions of Gases and Aerosols from Nature

832   version 2.1 (MEGAN2.1): an extended and updated framework for modeling biogenic

833   emissions. *GeoSci. Model Dev*. **5**, 1471-1492 (2012).

834   66. Emmerson, K.M., Palmer, P.I., Thatcher, M., Haverd, V. and Guenther, A.B.

835   Sensitivity of isoprene emissions to drought over south-eastern Australia: Integrating

836   models and satellite observations of soil moisture, *Atmos. Environ*. **209**, 112-124

837   (2019).

838   67. Kännaste, A., Copolovici, L. and Niinemets, Ü. Gas chromatography mass-

839   spectrometry method for determination of biogenic volatile organic compounds

840   emitted by plants. In: Plant isoprenoids: methods and protocols. Eds. M. Rodríguez-

841   Concepción, Humana Press, New York. pp. 161-169 (2014).

842   68. Tholl, D. *et al*. Practical approaches to plant volatile analysis. *Plant J*. **45**, 540 – 560

843   (2006).

844   69. Li, T., Holst, T., Michelsen, A. and Rinnan, R. Amplification of plant volatile defense

845   against insect herbivory in a warming Arctic tundra. *Nat. Plants* **5**, 568-475 (2019).

846   70. Johnsen, L.G., Skou, P.B., Khakimov, B., and Bro, R. Gas chromatography – mass

847   spectrometry data processing made easy. *J. Chromatogr. A*. **1503**, 57-64 (2017).

848   71. Keith, H. *et al*. Multiple measurements constrain estimates of net carbon exchange by

849   a *Eucalyptus* forest. *Agric. For. Meteorol.* **149**, 535-558 (2009).

850   72. Bates, D., Machler, M., Bolker, B.M., and Walker, S.C. Fitting linear mixed-effects

851   models using lme4. *J. Stat. Softw*. **67**, 1-48 (2015).

852   73. R Core Team. R: A language and environment for statistical computing. R Foundation

853   for Statistical Computing, Vienna, Austria. URL https://www.R-project.org/ (2018).

854   74. Ouimette, A.P. *et al*. Accounting for carbon flux to mycorrhizal fungi may resolve

855   discrepancies in forest carbon budgets. *Ecosystems* https://doi.org/10.1007/s10021-

856   019-00440-3 (2019).

857   75. Harrison, I., Jones, P.D., Osborn, T.J. and Lister, D.H. Updated high-resolution grids

858   of monthly climatic observations – the CRU TS3.10 dataset. *Int. J. Climatol.* **34**, 623-

859   642 (2014).

860   76. Olson, D.M. *et al*. Terrestrial ecoregions of the world: a new map of life on Earth.

861   *BioScience* **51**, 933-938 (2001).

862   77. Jiang, M., Felzer, B.S., Nielsen, U.N. and Medlyn, B.E. Biome-specific climatic space

863   defined by temperature and precipitation predictability. *Global Ecol. Biogeogr.* **26**,

864   1270-1282 (2017).

865   78. Scarascia-Mugnozza, G. *et al*. Response to elevated CO_2 of a short rotation,

866   multispecies Poplar plantation: the POPFACE/EUROFACE experiment. In Managed

867   Ecosystems and CO_2. Eds. Nösberger, J., *et al*. Berlin, Heidelberg, New York:

868   Springer Verlag. pp 173–195 (2006).

869   79. Linden, S. NPP Boreal Forest: Flakaliden, Sweden, 1986-1996, R1. Data set.

870   Available on-line [http://daac.ornl.gov] from Oak Ridge National Laboratory

871   Distributed   Active   Archive   Center,   Oak   Ridge,   Tennessee,   USA.

872   DOI:10.3334/ORNLDAAC/201 (2013).

873   80. Anderson-Teixeira, K.J. *et al.* ForC: a global database of forest carbon stock and

874   fluxes. *Ecology* **99**, 1507-1507 (2018).

875   81. Shangguan, W. Dai, Y., Duan, Q., Liu, B. and Yuan, H. A global soil data set for

876   earth system modelling. *J. Adv. Model Earth Sys*. **6**, 249-263 (2014).

877   82. Yang, X., Post, W.M., Thornton, P.E. and Jain, A. Global gridded soil phosphorus

878   distribution   maps   at   0.5-degree   resolution.   Data   set.   Available   on-line

879   [http://daac.ornl.gov]   from   Oak   Ridge   National   Laboratory   Distributed   Active

880   Archive   Center,   Oak   Ridge,   Tennessee,   USA.

881   http://dx.doi.org/10.3334/ORNLDAAC/1223 (2014).

882

Author contributions

MJ, BEM, RAD and JED designed the synthesis, compiled the data, and performed the analyses. MJ, BEM, JED, RAD, ICA, CVMB, MMB, YC, LC-G, LC, KYC, BMDS, SLF, ANG, TEG, SH, SNJ, AK, CAM, KM, BDM, LN, EHJN, UNN, ÜN, NJN, RO-H, VSP, EP, JP, JP, JRP, SAP, PBR, AAR, MR, RR, PR, RLS, BKS, BS, MGT, JKMW, AW-K, JY and DSE collected data and contributed to data analyses. MJ performed data assimilation analysis, with contributions from MGDK and BEM. JY and BEM performed the MAESPA model simulations, with contributions from MGDK and RAD. JED and AAR performed soil respiration gap-filling and modelling. KME performed the MEGAN model simulation. MJ and LC-G conceptualized Figure 1, and LC-G implemented the graphic design. MJ wrote the initial manuscript, with significant input from BEM, JED, BS, PBR, SZ, MGDK, MGT and DSE. All authors edited and approved the manuscript.

Competing financial interests

None declared.

Materials and Correspondence

Correspondence should be directed to MJ (m.jiang@westernsydney.edu.au) and BEM (b.medlyn@westernsydney.edu.au).

924   **Figure legend**

925

926   **Figure 1. A comprehensive carbon budget under ambient and elevated CO_2 treatment**

927   **in a mature forest ecosystem.** Diamond boxes are gross primary production for overstorey

928   (GPP_o) and understorey (GPP_u), respectively. Squared boxes are average carbon stocks over

929   the experimental period (C_{pools}, g C m^{-2}), including overstorey leaf (C_{ol}), stem (C_{stem}), coarse

930   root (C_{croot}), fine root (C_{froot}), intermediate root (C_{iroot}), understorey aboveground (C_{ua}), leaf

931   litter (C_{lit}), soil (C_{soil}), microbe (C_{micr}), aboveground insect (C_{ins}), and mycorrhizae (C_{myco}).

932   Unboxed variables are carbon fluxes (g C m^{-2} yr^{-1}), including net primary production of

933   overstorey leaf (NPP_{ol}), stem (NPP_{stem}), coarse root (NPP_{croot}), fine root (NPP_{froot}),

934   intermediate root (NPP_{iroot}), and understorey aboveground (NPP_{ua}), overstorey leaf

935   consumption by insects (NPP_{ins}), respiration fluxes of overstorey leaf (R_{ol}), stem (R_{stem}), root

936   (R_{root}), understorey aboveground (R_{ua}), growth (R_{grow}), insect (R_{ins}), heterotroph (R_{hetero}), and

937   soil (R_{soil}), and volatile carbon emission (VC), frass production (Frass), dissolved organic

938   carbon (DOC), and soil methane net uptake (CH_4). Solid arrow lines are fluxes entering a

939   pool, dotted arrow lines are fluxes leaving a pool. The changes in each carbon pool over time

940   (ΔC_{pools}, g C m^{-2} yr^{-1}) are reported in Extended Data Figure 6. Blue italic values are means ±

941   one standard deviation of the ambient CO_2 treatment (n=3), whereas red values are means ±

942   one standard deviation of the elevated CO_2 treatment (n=3). All values are normalized by a

943   linear mixed-model with plot-specific pre-treatment leaf area index as a covariate to account

944   for pre-existing differences. A summary of variable definitions and data availability is

945   provided   in   Extended   Data   Table   1.

946 **Figure 2. The fate of additional carbon fixed under elevated CO_2 (eCO_2) in a mature**

947 **forest ecosystem. a)** Column **"GPP"** represents the total eCO_2-induced increases in

948 overstorey and understorey gross primary production (GPP_o and GPP_u, respectively), "NPP +

949 R_a" represents the sum of net primary production and autotrophic respiration response, "R +

950 ΔC_{pools}" represents the sum of ecosystem respiration and change in carbon storage response.

951 **b)** The relative contributions of individual NPP fluxes to the aggregated NPP response to

952 eCO_2, including NPP responses of overstorey leaf (NPP_{ol}), twigs, barks and seeds (NPP_{other}),

953 fine root (NPP_{froot}), and understorey aboveground (NPP_{ua}); **c)** The relative contributions of

954 individual respiratory fluxes to the aggregated R response to eCO_2, including respiration

955 responses of stem (R_{stem}), root (R_{root}), understorey aboveground (R_{ua}), growth (R_{grow}), and soil

956 heterotroph (R_{hetero}); and **d)** The relative contributions of individual change in carbon storage

957 to the aggregated ΔC_{pools} response to eCO_2, including changes in pool of stem (ΔC_{stem}),

958 understorey aboveground (ΔC_{ua}), fine root (ΔC_{froot}), leaf litter (ΔC_{lit}), and soil (ΔC_{soil}).

959 Variables with an absolute mean CO_2 effect of < 5 g C m^{-2} yr^{-1} are not reported in the bar

960 chart for better visual clarification. Individual CO_2 responses are reported in Extended Data

961 Figure 5. Each color represents the CO_2 response of a flux variable, the point indicates the net

962 sum of all variables for a column, and the grey error bar represents one standard deviation of

963 the estimated column sum at the plot-level (see Methods). The CO_2 effect is estimated using a

964 linear mixed-model analysis with plot-specific pre-treatment leaf area index as a covariate to

965 account for pre-existing differences (see Methods). The non-normalized response is provided

966 in Extended Data Figure 4, which generally agrees with findings present in this figure, but

967 with   larger   uncertainty.

968   **Figure 3. Estimates of net ecosystem production (NEP) under ambient and elevated CO_2**

969   **treatment at EucFACE.** Positive values indicate ecosystem net carbon uptake by the

970   ecosystem. "In - Out" calculates NEP based on the difference between total influxes and total

971   outfluxes. "NPP - R_{hetero}" calculates NEP based on the difference between net primary

972   production (NPP) and heterotrophic respiration (R_{hetero}). "ΔC_{pools}" derives NEP based on

973   incremental changes in all ecosystem carbon pools. Colored bars indicate treatment means

974   based on each method (n=3), with blue representing ambient and red representing elevated

975   CO_2 treatment. Individual dots are plot-level NEP, derived based on different methods (see

976   Methods). Values are normalized by a linear mixed-model with plot-specific pre-treatment

977   leaf area index as a covariate to account for pre-existing differences. Horizontal dotted line

978   indicates NEP equals zero. The inset figure includes an inferred production allocation flux to

979   mycorrhizal fungi (NPP_{myco}) based on data assimilation (Methods), which affected NEP

980   estimates based on the NPP – R_{hetero} method only.

981 **Extended Data Table 1. Definition and data availability of variables.** Data availability

982 includes start and end year of data included in this study. Time points indicate the number of

983 data collections over the available data period. Within plot sub-replicate indicate the number

984 of replicates within each treatment plot. The detailed methods for estimating each variable is

985 provided in the Method section.

Variable		Data coverage			
Name	Symbol	Start year	End year	Time points	Within plot sub-replicate (plot^{-1})
Specific Leaf Area	SLA	2013	2016	50	3
Leaf Area Index	LAI	2012	2016	303	1
Soil bulk density	BK	2017	2017	2	3
Diameter at breast height	DBH	2013	2016	4	Individual tree
Overstorey leaf pool	C_{ol}	2012	2016	303	1
Understorey aboveground pool	C_{ua}	2015	2016	16	4
Overstorey stem C pool	C_{stem}	2013	2016	4	Individual tree
Fine root C pool	C_{froot}	2014	2016	7	4
Intermediate root C pool	C_{iroot}	2014	2016	7	4
Coarse root C pool	C_{croot}	2013	2016	4	Individual tree
Forest floor leaf litter C pool	C_{lit}	2013	2016	46	-
Microbial C pool	C_{micr}	2012	2015	15	4
Soil C pool	C_{soil}	2012	2014	11	4

Mycorrhizal C pool	C_{myco}	2015	2015	3	-
Insect C pool (aerial)	C_{ins}	2013	2016	43	8
Insect C pool (understorey)	C_{ins}	2014	2015	5	2
Overstorey gross primary production	GPP_o	2013	2016	Annual	1
Understorey gross primary production	GPP_u	2013	2016	Annual	1
Overstorey leaf respiration	R_{ol}	2013	2016	Annual	1
Understorey leaf respiration	R_{ua}	2013	2016	Annual	1
Stem respiration	R_{stem}	2012	2016	Daily	3
Root respiration	R_{root}	2012	2015	Daily	-
Methane net flux	CH_4	2013	2016	35	7
Volatile C emission flux	VC	2013	2016	Daily	1
Insect herbivore respiration	R_{ins}	2012	2014	22	-
Dissolved organic C loss flux	DOC	2012	2014	12	4
Soil respiration	R_{soil}	2012	2015	Daily	8
Growth respiration	R_{grow}	2012	2016	Annual	1
Overstorey leaf net primary production	NPP_{ol}	2012	2016	49	8
Stem net primary production	NPP_{stem}	2012	2016	4	Individual tree
Fine root net primary production	NPP_{froot}	2014	2016	6	4
Intermediate root net primary production	NPP_{iroot}	2014	2016	6	4

Coarse root net primary production	NPP$_{croot}$	2012	2016	4	Individual tree
Other net primary production (sum of twigs, bark, seeds)	NPP$_{other}$	2012	2016	49	8
Twig net primary production	NPP$_{twig}$	2012	2016	49	8
Bark net primary production	NPP$_{bark}$	2012	2016	49	8
Seed net primary production	NPP$_{seed}$	2012	2016	49	8
Understorey aboveground net primary production	NPP$_{ua}$	2015	2016	3	4
Frass production	Frass	2012	2014	22	8
Heterotrophic respiration	R$_{hetero}$	2012	2016	Daily	8
Overstorey leaf insect consumption flux	NPP$_{ins}$	2012	2014	22	-

986

987 **Extended Data Table 2. Carbon (C) fraction used to convert from biomass into C**

988 **content.**

Variable	Symbol	Mean value	Data source
C fraction of overstorey leaf pool	f_{ol}	0.5	EucFACE data
C fraction of understorey aboveground pool	f_{ua}	0.456	EucFACE data
C fraction of stem pool	f_{stem}	0.445 (ambient plots) 0.448 (elevated plots)	EucFACE data
C fraction of coarse root pool	f_{croot}	0.445 (ambient plots) 0.448 (elevated plots)	Assumed the same as f_{stem}
C fraction of fine root pool	f_{froot}	0.40 (ambient plots) 0.42 (elevated plots)	EucFACE data
C fraction of intermediate root pool	F_{iroot}	0.40 (ambient plots) 0.42 (elevated plots)	Assumed the same as f_{froot}
C fraction of overstorey leaflitter pool	f_{lit}	0.5	EucFACE data
C fraction of aboveground insect pool	f_{ins}	0.5	Ref 49
C fraction of frass production	f_{frass}	0.53	EucFACE data
C fraction of microbial pool	f_{micr}	0.534 (ambient plots) 0.493 (elevated plots)	EucFACE data
C fraction of mycorrhizal pool	f_{myco}	0.534 (ambient plots) 0.493 (elevated plots)	Assumed the same as f_{micr}
C fraction of soil pool	f_{soil}	0.016 (ambient plots) 0.017 (elevated plots)	EucFACE data
C fraction of twigs, barks and seeds production	f_{other}	0.5	Assumed

989

990

991   **Extended Data Figure 1. The *Eucalyptus* Free Air Carbon dioxide Enrichment**

992   **experiment facility (EucFACE)**. **a)** View of the forest and facility from above (photo credit:

993   David S. Ellsworth), **b)** view of the understorey vegetation and infrastructure inside a plot

994   (photo credit: Mingkai Jiang), and **c)** view from below of the canopy structure and the crane

995   (photo credit: Mingkai Jiang).

996

997 **Extended Data Figure 2. Mean annual temperature (MAT) and mean annual**

998 **precipitation (MAP) for major forest biomes and a selected list of tree-based elevated**

999 **CO$_2$ experiments.** Gridded temperature and precipitation data were obtained from the

1000 Climate Research Unit (CRU) monthly dataset at 0.5 resolution[75]. Global biome boundaries

1001 and definitions were taken from Ref 76 and were spatially aggregated onto the CRU

1002 resolution, following Ref 77. The major forest biomes are defined as: tropical and subtropical

1003 moist broadleaf forests; tropical and subtropical dry broadleaf forests; tropical and

1004 subtropical coniferous forest; temperate broadleaf and mixed forests; temperate coniferous

1005 forests; boreal forests/taiga; and Mediterranean forests, woodlands, and scrub. The list of

1006 elevated CO$_2$ experiments includes 7 Free Air CO$_2$ Enrichment experiments (FACE) and a

1007 Whole-Tree Chamber experiment (WTC), namely: EucFACE, DukeFACE, ORNLFACE,

1008 AspenFACE, PopFACE, WebFACE, BiForFACE, and FlakalidenWTC. The site-specific

1009 climate, tree age and net primary production (NPP) under ambient CO$_2$ treatment were

1010 collected from Ref 3, 9, 10, 11, 78 and 79. The top inset figure compares global forest NPP

1011 against standing age using data collected from Ref 80. We included data with forest age <

1012 500 years, and the NPP reported in Ref 80 included both overstorey and understorey. The

1013 bottom inset figure compares soil total nitrogen and labile phosphorus across the eCO$_2$

1014 experiments. Soil total nitrogen was extracted from Ref 81 using spatial coordinates of each

1015 experiment, while soil labile phosphorus was spatially extracted from Ref 82. The two dotted

1016 lines indicates N:P ratios of 20:1 and 100:1, respectively.

Extended Data Figure 3. Estimates of (a and b) gross primary production (GPP) and (c and d) soil respiration (R_{soil}) based on different methods for both (a and c) ambient and (b and d) elevated CO$_2$ treatment at EucFACE. For estimates of GPP, we compared the model simulated total GPP of overstorey and understorey (GPP$_o$ and GPP$_u$, respectively), with the sum of data-driven estimates of net primary production (NPP) and autotrophic respiration (R_a), which include NPP of overstorey leaf (NPP$_{ol}$), stem (NPP$_{stem}$), fine root (NPP$_{froot}$), intermediate root (NPP$_{iroot}$), coarse root (NPP$_{croot}$), twigs, barks and seeds (NPP$_{other}$), understorey aboveground (NPP$_{ua}$), leaf consumption by insects (NPP$_{ins}$), and respiratory fluxes of overstorey leaf (R_{ol}), stem (R_{stem}), root (R_{root}), understorey aboveground (R_{ua}), growth (R_{grow}), and volatile carbon emission (VC). For estimates of R_{soil}, we compared direct estimates of R_{soil} scaled up from soil chamber measurements, with the sum of litterfall and independent estimates of root respiration (Litter + R_{root}), assuming no net change in soil carbon stock over time. Here litterfall was inferred based on NPP of overstorey leaf (NPP$_{ol}$), fine root (NPP$_{froot}$), intermediate root (NPP$_{iroot}$), twigs, barks and seeds (NPP$_{other}$), understorey aboveground (NPP$_{ua}$), and frass production (Frass). These evaluations provide independent mass balance checks of the estimated ecosystem carbon budget. Each color represents a flux variable. Dotted point and vertical line represent treatment mean and standard deviation based on plot-level estimates of the aggregated flux (n=3). Values were normalized by a linear mixed-model with pre-treatment leaf area index as a covariate to account for pre-existing differences.

Extended Data Figure 4. The fate of additional carbon fixed under elevated CO_2 (eCO_2) in a mature forest ecosystem (non-normalized analysis case). a) Column **"GPP"** represents the total eCO_2 induced increase in overstorey and understorey gross primary production (GPP_o and GPP_u, respectively), column "NPP + R_a" represents the sum of net primary production and autotrophic respiration eCO_2 response, and column "R + ΔC_{pools}" represents the sum of ecosystem respiration and carbon storage eCO_2 response. **b)** The relative contributions of individual NPP fluxes to the aggregated NPP response to eCO_2, including overstorey leaf (NPP_{ol}), stem (NPP_{stem}), fine root (NPP_{froot}) and understorey aboveground (NPP_{ua}). **c)** The relative contributions of individual respiratory fluxes to the aggregated R response to eCO_2, including overstorey leaf (R_{ol}), stem (R_{stem}), root (R_{root}), understorey aboveground (R_{ua}), and heterotroph (R_{hetero}). **d)** The relative contributions of individual change in carbon storage to the aggregated ΔC_{pools} response to eCO_2, including stem (ΔC_{stem}), fine root (ΔC_{froot}), leaflitter (ΔC_{lit}), understorey aboveground (ΔC_{ua}), and soil (ΔC_{soil}). Variables with an average CO_2 effect of < 5 g C m^{-2} yr^{-1} were excluded from the figure for better visual clarification. Each color represents a flux variable, point indicates the net sum of all variables for a column, and the grey confidence interval represents plot-level standard deviation (n=3) of the estimated column sum.

1054

1055 **Extended Data Figure 5. CO_2 treatment effect (g C m^{-2} yr^{-1}) for all ecosystem fluxes at**

1056 **EucFACE. a)** The CO_2 response of gross ecosystem carbon uptake, including gross primary

1057 production of overstorey (GPP_o) and understorey (GPP_u), and soil methane uptake (CH_4). **b)**

1058 The eCO_2 response of annual incremental change in carbon pool (ΔC_{pools}), including

1059 overstorey leaf (ΔC_{ol}), stem (ΔC_{stem}), coarse root (ΔC_{croot}), fine root (ΔC_{froot}), intermediate

1060 root (ΔC_{iroot}), understorey aboveground (ΔC_{ua}), leaf litter (ΔC_{lit}), soil (ΔC_{soil}), microbe

1061 (ΔC_{micr}), aboveground insect (ΔC_{ins}), and mycorrhizae (ΔC_{myco}). **c)** The eCO_2 response of net

1062 primary production (NPP), including overstorey leaf (NPP_{ol}), stem (NPP_{stem}), coarse root

1063 (NPP_{croot}), fine root (NPP_{froot}), intermediate root (NPP_{iroot}), understorey aboveground (NPP_{ua}),

1064 twigs, barks and seeds (NPP_{other}), and leaf insect consumption (NPP_{ins}). **d)** The eCO_2

1065 response of ecosystem respiration (R) and other out-going flux, including respiration fluxes

1066 of overstorey leaf (R_{ol}), stem (R_{stem}), root (R_{root}), understorey aboveground (R_{ua}), growth

1067 (R_{grow}), insect (R_{ins}), heterotroph (R_{hetero}), and soil (R_{soil}), and volatile carbon emission (VC)

1068 and dissolved organic carbon leaching (DOC). Dots and grey bars represent means and

1069 standard deviations of the CO_2 treatment difference, predicted by a linear mixed-model with

1070 plot-specific pre-treatment leaf area index as a covariate. Red dots indicate negative means

1071 and blue dots indicate positive means. Dashed lines indicate change of scale along the x-axis.

1072

1073 **Extended Data Figure 6. Estimates of incremental change in carbon pool averaged over**

1074 **the experimental period under ambient (aCO₂) and elevated CO₂ (eCO₂) treatment**

1075 **effect at EucFACE (ΔC_{pools}, g C m^{-2} yr^{-1}).** The ΔC_{pools} variables are overstorey leaf (ΔC_{ol}),

1076 stem (ΔC_{stem}), coarse root (ΔC_{croot}), fine root (ΔC_{froot}), intermediate root (ΔC_{iroot}), understorey

1077 aboveground (ΔC_{ua}), leaf litter (ΔC_{lit}), soil (ΔC_{soil}), microbe (ΔC_{micr}), aboveground insect

1078 (ΔC_{ins}), and mycorrhizae (ΔC_{myco}). Colored bars and black lines represent means and standard

1079 deviations for each treatment, with blue represents aCO₂ and red represents eCO₂ treatment.

1080 Dashed lines indicate change of scale along the x-axis.

1081 **Extended Data Figure 7. Fitted carbon cycle parameters to trace the fate of the**

1082 **additional carbon under elevated CO_2 at EucFACE.** Parameters were estimated by

1083 Markov Chain Monte Carlo (MCMC) fitting algorithm, assuming a simplified carbon cycle

1084 framework based on data collected from EucFACE. Details of the MCMC approach can be

1085 found in the Methods. Plot-level gross primary production (GPP), autotrophic respiration (R_a),

1086 heterotrophic respiration (R_{hetero}), carbon pools of leaf (C'_{leaf}), wood (C'_{wood}), root (C'_{root}),

1087 mycorrhizae (C'_{myco}), microbe (C'_{micr}), and soil (C'_{soil}), and the corresponding change in

1088 pools were used to constrain the model fitting. Net primary production (NPP) was derived as

1089 the difference of GPP and R_a. Carbon use efficiency (CUE') was calculated as NPP/GPP; it

1090 differs from the value given in the main text owing to the contribution of NPP allocated to

1091 mycorrhizae (NPP_{myco}). We fitted two carbon pools (C'_{aglit} and C'_{bglit}), four allocation

1092 coefficients (a_{leaf}, a_{wood}, a_{root}, and a_{myco}), six turnover rates (τ_{leaf}, τ_{root}, τ_{myco}, τ_{bglit}, τ_{micr}, and

1093 τ_{soil}), and three fractional coefficients (f'_{aglit}, f'_{bglit}, and f'_{micr}) using MCMC algorithm. The

1094 fractional coefficients indicate the fraction of carbon leaving one pool that enters the

1095 subsequent   pool,   with   the   remainder   respired   as R_{hetero}.

1096

1097 **Extended Data Figure 8. Data-model intercomparison of some key carbon cycle**

1098 **parameters, under ambient (aCO$_2$) and elevated CO$_2$ (eCO$_2$).** Parameters include: **a)**

1099 allocation coefficients to leaf, wood, root and other, **b)** turnover rates of leaf, root,

1100 aboveground litter (Aglit), belowground litter (Bglit), and **c)** turnover rate of soil. Models

1101 include: Community Atmosphere Biosphere Land Exchange (CABL), Community Land

1102 Model 4 (CLM4), Community Land Model with a phosphorus component (CLMP), Generic

1103 Decomposition And Yield (GDAY), Lund-Potsdam-Jena General Ecosystem Simulator

1104 (LPJX), Orchidee-C-N (OCNX), and Sheffield Dynamic Global Vegetation Model (SDVM).

1105 The model output was generated as part of the model ensemble predictions made in advance

1106 of the experiment reported in Ref 17 for EucFACE. Data-based uncertainties were estimated

1107 using the Markov Chain Monte Carlo data assimilation algorithm, with error bars indicating

1108 one standard deviation. Allocation to other in the data refers to the allocation to mycorrhizal

1109 production, whereas it refers to the allocation to reproductive carbon pool in some models.

1110
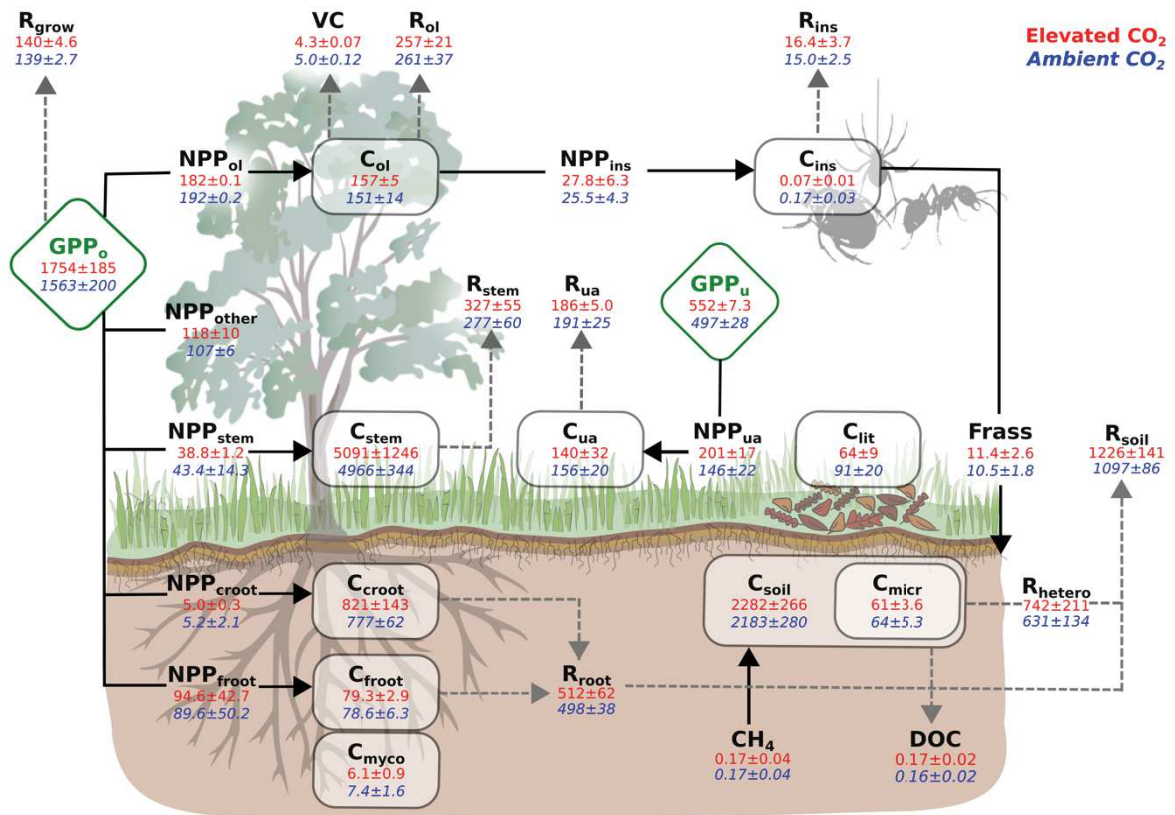
Figures

Figure 1. A comprehensive carbon budget under ambient and elevated CO_2 treatment in a mature forest ecosystem. Diamond boxes are gross primary production for overstorey (GPP_o) and understorey (GPP_u), respectively. Squared boxes are carbon stocks (gCm^{-2}), including overstorey leaf (C_{ol}), stem (C_{stem}), coarse root (C_{croot}), fineroot (C_{froot}), understorey aboveground (C_{ua}), leaf litter (C_{lit}), soil (C_{soil}), microbe (C_{micr}), aboveground insect (C_{ins}), and mycorrhizae (C_{myco}). Unboxed variables are carbon fluxes ($gCm^{-2}yr^{-1}$), including net primary production of overstorey leaf (NPP_{ol}), stem (NPP_{stem}), coarse root (NPP_{croot}), fineroot (NPP_{froot}), and understorey aboveground (NPP_{ua}), overstorey leaf consumption by insects (NPP_{ins}), respiration fluxes of overstorey leaf (R_{ol}), stem (R_{stem}), root (R_{root}), understorey aboveground (R_{ua}), growth (R_{grow}), insect (R_{ins}), heterotroph (R_{hetero}), and soil (R_{soil}), and volatile carbon emission (VC), frass production (Frass), dissolved organic carbon (DOC), and soil methane net

775   uptake (CH_4). Solid arrow lines are fluxes entering a pool, dotted arrow lines are fluxes leaving

776   a pool. Blue italic values are means ± one standard deviation of the ambient CO_2 treatment

777   (n=3), whereas red values are means ± one standard deviation of the elevated CO_2 treatment

778   (n=3). All values are normalized by a linear mixed-model with plot-specific pre-treatment leaf

779   area index as a covariate to account for pre-existing differences. Summary of variable

780   definitions and data availability is provided in Extended Data Table 1.
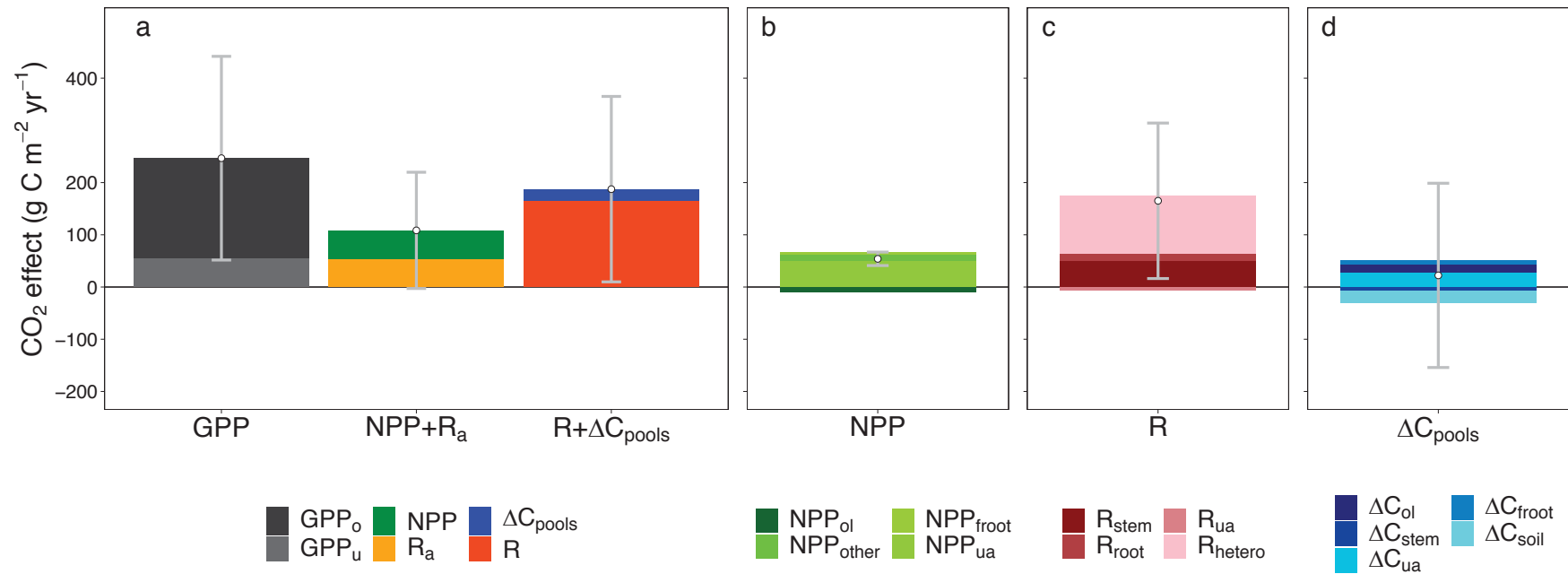
Figure 2. The fate of additional carbon fixed under elevated CO_2 (eCO_2) in a mature forest ecosystem. a) Column "GPP" represents the total

eCO_2-induced increases in overstorey and understorey gross primary production (GPP_o and GPP_u, respectively), "NPP + R_a" represents the sum

of net primary production and autotrophic respiration response, "R + ΔC_{pools}" represents the sum of ecosystem respiration and carbon storage

response. **b)** The relative contributions of individual NPP fluxes to the aggregated NPP response to eCO_2, including NPP responses of overstorey

leaf (NPP_{ol}), twigs, barks and seeds (NPP_{other}), fineroot (NPP_{froot}), and understorey aboveground (NPP_{ua}); **c)** The relative contributions of individual

respiratory fluxes to the aggregated R response to eCO_2, including respiration responses of stem (R_{stem}), root (R_{root}), understorey aboveground

789   (R_{ua}), and soil heterotroph (R_{hetero}); and **d)** The relative contributions of individual change in carbon storage to the aggregated ΔC_{pools} response to

790   eCO$_2$, including changes in pool of overstorey leaf (ΔC_{ol}), stem (ΔC_{stem}), understorey aboveground (ΔC_{ua}), fineroot (ΔC_{froot}), and soil (ΔC_{soil}).

791   Variables with an absolute mean CO$_2$ effect of < 5 gCm^{-2}yr^{-1} are excluded from the figure for better visual clarification. Individual CO$_2$ responses

792   are reported in Extended Data Figure 4. Each color represents the CO$_2$ response of a flux variable, point indicates the net sum of all variables for

793   a column, and the grey error bar represents one standard deviation of the estimated column sum at the plot-level (see Methods). The CO$_2$ effect is

794   estimated using a linear mixed-model analysis with plot-specific pre-treatment leaf area index as a covariate to account for pre-existing differences

795   (see Methods). The un-normalized response is provided in Extended Data Figure 3, which generally agrees with findings present in this figure, but

796   with less statistical precision.

Figure 3. Estimates of net ecosystem production (NEP) under ambient and elevated CO_2 treatment at EucFACE. Positive values indicate ecosystem net carbon uptake by the ecosystem. "In - Out" calculates NEP based on the difference between total influxes and total outfluxes. "NPP - R_{hetero}" calculates NEP based on the difference between net primary production (NPP) and heterotrophic respiration (R_{hetero}). "ΔC_{pools}" derives NEP based on incremental changes in all ecosystem carbon pools. Colored bars indicate treatment means based on each method (n=3), with blue representing ambient and red representing elevated CO_2

806   treatment. Individual dots are plot-level NEP, derived based on different methods (see

807   Methods). Values are normalized by a linear mixed-model with plot-specific pre-treatment leaf

808   area index as a covariate to account for pre-existing differences. Horizontal dotted line indicates

809   NEP equals zero.

810 **Extended Data Table 1. Definition and data availability of variables.** Data availability

811 includes start and end year of data included in this study. Time points indicate the number of

812 data collections over the available data period. Within plot sub-replicate indicate the number

813 of replicates within each treatment plot. The detailed methods for estimating each variable is

814 provided in the Method section.

Variable		Data coverage			
Name	**Symbol**	**Start year**	**End year**	**Time points**	**Within plot sub-replicate (plot^{-1})**
Specific Leaf Area	SLA	2013	2016	50	3
Leaf Area Index	LAI	2012	2016	303	1
Soil bulk density	BK	2017	2017	2	3
Diameter at breast height	DBH	2013	2016	4	Individual tree
Overstorey leaf pool	C_{ol}	2012	2016	303	1
Understorey aboveground pool	C_{ua}	2015	2016	16	4
Overstorey stem C pool	C_{stem}	2013	2016	4	Individual tree
Fine root C pool	C_{froot}	2014	2016	6	4
Coarse root C pool	C_{croot}	2013	2016	4	Individual tree
Forest floor leaf litter C pool	C_{lit}	2013	2016	46	-
Microbial C pool	C_{micr}	2012	2015	15	4
Soil C pool	C_{soil}	2012	2014	11	4

Mycorrhizal C pool	C_{myco}	2015	2015	3	-
Insect C pool (aeriel)	C_{ins}	2013	2016	43	8
Insect C pool (ground dwelling)	C_{ins}	2013	2015	5	4
Overstorey gross primary production	GPP_o	2013	2016	Annual	1
Understorey gross primary production	GPP_u	2013	2016	Annual	1
Overstorey leaf respiration	R_{ol}	2013	2016	Annual	1
Understorey leaf respiration	R_{ua}	2013	2016	Annual	1
Stem respiration	R_{stem}	2012	2016	Daily	3
Root respiration	R_{root}	2012	2015	Daily	-
Methane net flux	CH_4	2013	2016	35	7
Volatile C emission flux	VC	2013	2016	Daily	1
Insect herbivore respiration	R_{ins}	2012	2014	22	-
Dissolved organic C loss flux	DOC	2012	2014	12	4
Soil respiration	R_{soil}	2012	2015	Daily	8
Growth respiration	R_{grow}	2012	2016	Annual	1
Overstorey leaf net primary production	NPP_{ol}	2012	2016	49	8
Stem net primary production	NPP_{stem}	2012	2016	4	Individual tree

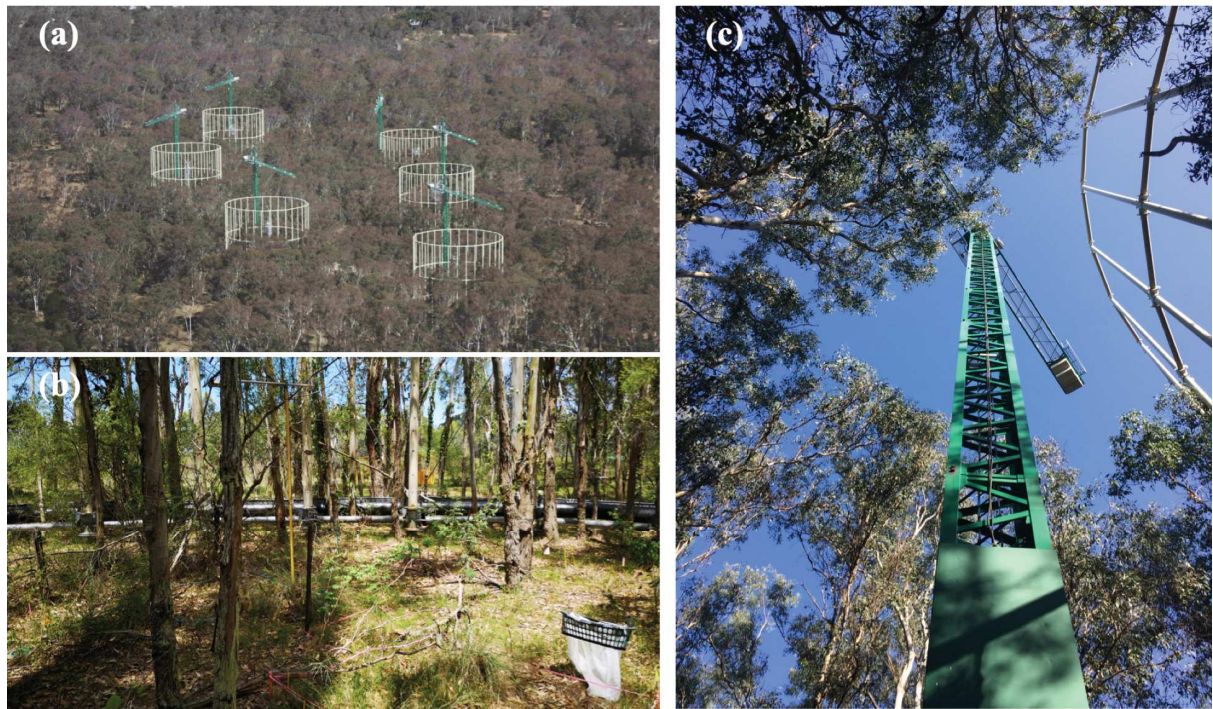| Fine root net primary production	NPP_{froot}	2014	2016	5	4
Coarse root net primary production	NPP_{croot}	2012	2016	4	Individual tree
Other net primary production (sum of twigs, bark, seeds)	NPP_{other}	2012	2016	49	8
Twig net primary production	NPP_{twig}	2012	2016	49	8
Bark net primary production	NPP_{bark}	2012	2016	49	8
Seed net primary production	NPP_{seed}	2012	2016	49	8
Understorey aboveground net primary production	NPP_{ua}	2015	2016	3	4
Frass production	Frass	2012	2014	22	8
Heterotrophic respiration	R_{hetero}	2012	2016	Daily	8
Overstorey leaf insect consumption flux	NPP_{ins}	2012	2014	22	-

815

Extended Data Table 2. Carbon (C) fraction used to convert from biomass into C content.

Variable	Symbol	Mean value	Data source
C fraction of overstorey leaf pool	f_{ol}	0.5	EucFACE data
C fraction of understorey aboveground pool	f_{ua}	0.456	EucFACE data
C fraction of stem pool	f_{stem}	0.445 (ambient plots) 0.448 (elevated plots)	EucFACE data
C fraction of coarse root pool	f_{croot}	0.445 (ambient plots) 0.448 (elevated plots)	Assumed the same as f_{stem}
C fraction of fine root pool	f_{froot}	0.40 (ambient plots) 0.42 (elevated plots)	EucFACE data
C fraction of overstorey leaflitter pool	f_{lit}	0.5	EucFACE data
C fraction of aboveground insect pool	f_{ins}	0.5	Ref 48
C fraction of frass production	f_{frass}	0.53	EucFACE data
C fraction of microbial pool	f_{micr}	0.534 (ambient plots) 0.493 (elevated plots)	EucFACE data

|			
C fraction of mycorrhizal pool	f_{myco}	0.534 (ambient plots) 0.493 (elevated plots)	Assumed the same as f_{micr}
C fraction of soil pool	f_{soil}	0.016 (ambient plots) 0.017 (elevated plots)	EucFACE data
C fraction of twigs, barks and seeds production	f_{other}	0.5	Assumed

817

818

Extended Data Figure 1. The *Eucalyptus* free air carbon dioxide enrichment experiment facility (EucFACE). **a)** A spatial overview of the forest and the facility (photo credit: David S. Ellsworth), **b)** an overview of the understorey vegetation and infrastructure inside a plot (photo credit: Mingkai Jiang), and **c)** a bottom-up look of the canopy structure and the crane (photo credit: Mingkai Jiang).

824
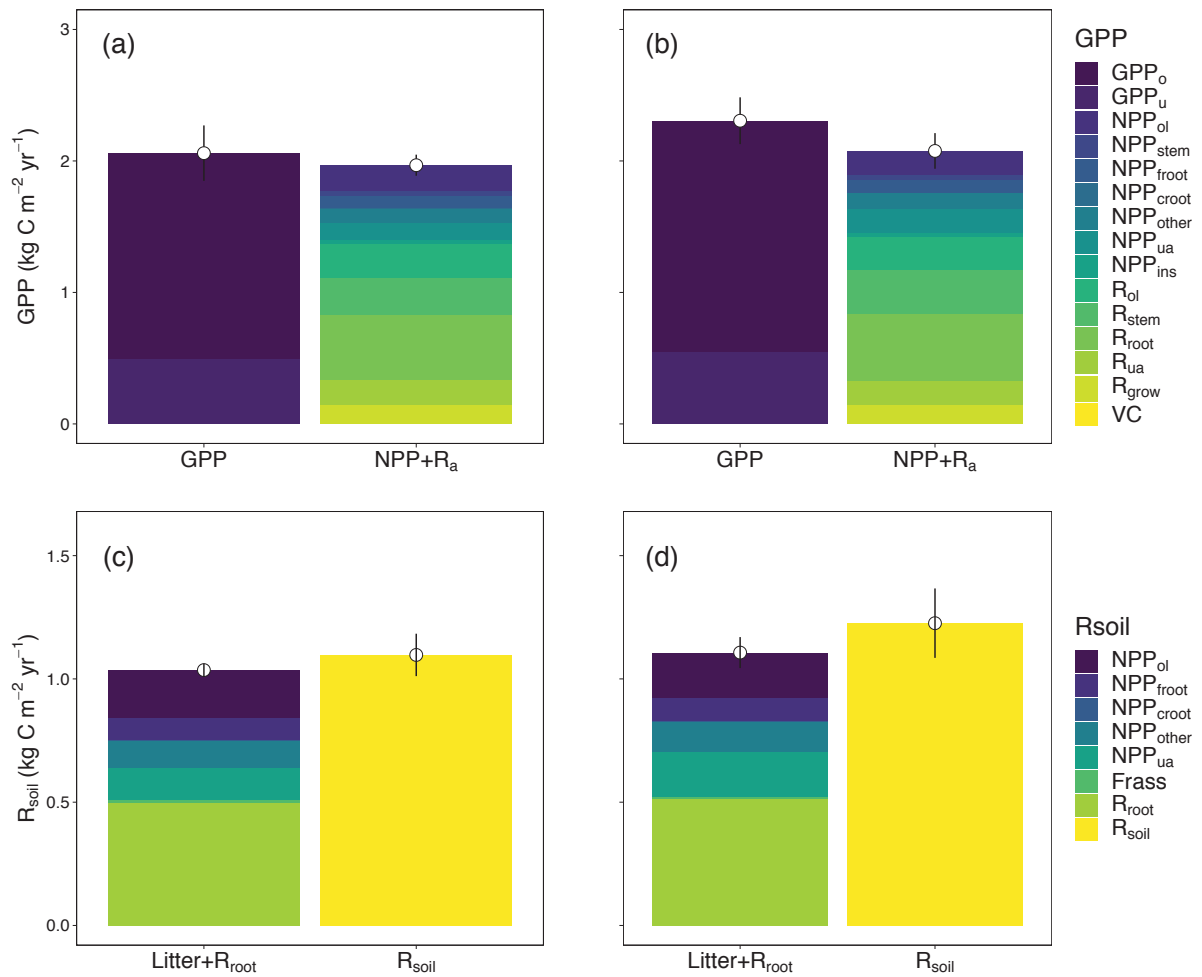
**Extended Data Figure 2. Estimates of (a and b) gross primary production (GPP) and (c and d) soil respiration (R_{soil}) based on different methods for both (a and c) ambient and (b and d) elevated CO_2 treatment at EucFACE.** For estimates of GPP, we compared the model simulated total GPP of overstorey and understorey (GPP_o and GPP_u, respectively), with the sum of data-driven estimates of net primary production (NPP) and autotrophic respiration (R_a), which include NPP of overstorey leaf (NPP_{ol}), stem (NPP_{stem}), fineroot (NPP_{froot}), coarse root (NPP_{croot}), twigs, barks and seeds (NPP_{other}), understorey aboveground (NPP_{ua}), leaf consumption by insects (NPP_{ins}), and respiratory fluxes of overstorey leaf (R_{ol}), stem (R_{stem}), root (R_{root}), understorey aboveground (R_{ua}), growth (R_{grow}), and volatile carbon emission (VC). For estimates of R_{soil}, we compared direct estimates of R_{soil} scaled up from soil chamber

837   measurements, with the sum of litterfall and independent estimates of root respiration (Litter +

838   R_{root}), assuming no net change in soil carbon stock over time. Here litterfall was inferred based

839   on NPP of overstorey leaf (NPP_{ol}), fineroot (NPP_{froot}), coarse root (NPP_{croot}), twigs, barks and

840   seeds (NPP_{other}), understorey aboveground (NPP_{ua}), and frass production (Frass). These

841   evaluations provide independent mass balance checks of the estimated ecosystem carbon

842   budget. Each color represents a flux variable. Dotted point and vertical line represent treatment

843   mean and standard deviation based on plot-level estimates of the aggregated flux (n=3). Values

844   were normalized by a linear mixed-model with pre-treatment leaf area index as a covariate to

845   account for pre-existing differences.
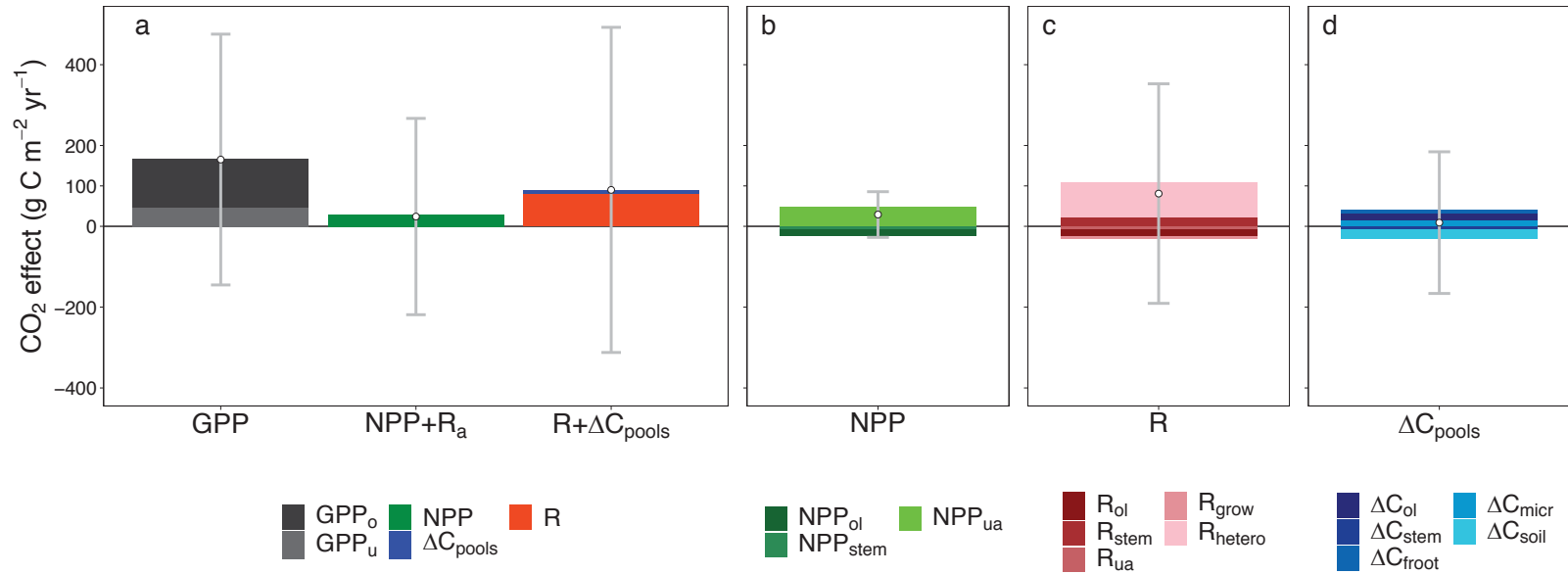
Extended Data Figure 3. The fate of additional carbon fixed under elevated CO_2 (eCO_2) in a mature forest ecosystem (non-normalized analysis case). a) Column "GPP" represents the total eCO_2 induced increase in overstorey and understorey gross primary production (GPP$_o$ and GPP$_u$, respectively), column "NPP + R$_a$" represents the sum of net primary production and autotrophic respiration eCO_2 response, and column "R + ΔC_{pools}" represents the sum of ecosystem respiration and carbon storage eCO_2 response. **b)** The relative contributions of individual NPP fluxes to the aggregated NPP response to eCO_2, including overstorey leaf (NPP$_{ol}$), stem (NPP$_{stem}$), and understorey aboveground (NPP$_{ua}$). **c)** The relative contributions of individual respiratory fluxes to the aggregated R response to eCO_2, including overstorey leaf (R$_{ol}$), stem (R$_{stem}$), understorey aboveground (R$_{ua}$), growth (R$_{grow}$), and heterotroph (R$_{hetero}$). **d)** The relative contributions of individual change in carbon storage to the aggregated ΔC_{pools} response to eCO_2, including overstorey leaf (ΔC_{ol}), stem (ΔC_{stem}), fineroot (ΔC_{froot}), microbe (ΔC_{micr}), and soil (ΔC_{soil}). Variables with an

855   average CO_2 effect of < 5 $gCm^{-2}yr^{-1}$ were excluded from the figure for better visual clarification. Each color represents a flux variable, point

856   indicates the net sum of all variables for a column, and the grey confidence interval represents plot-level standard deviation (n=3) of the estimated

857   column sum.
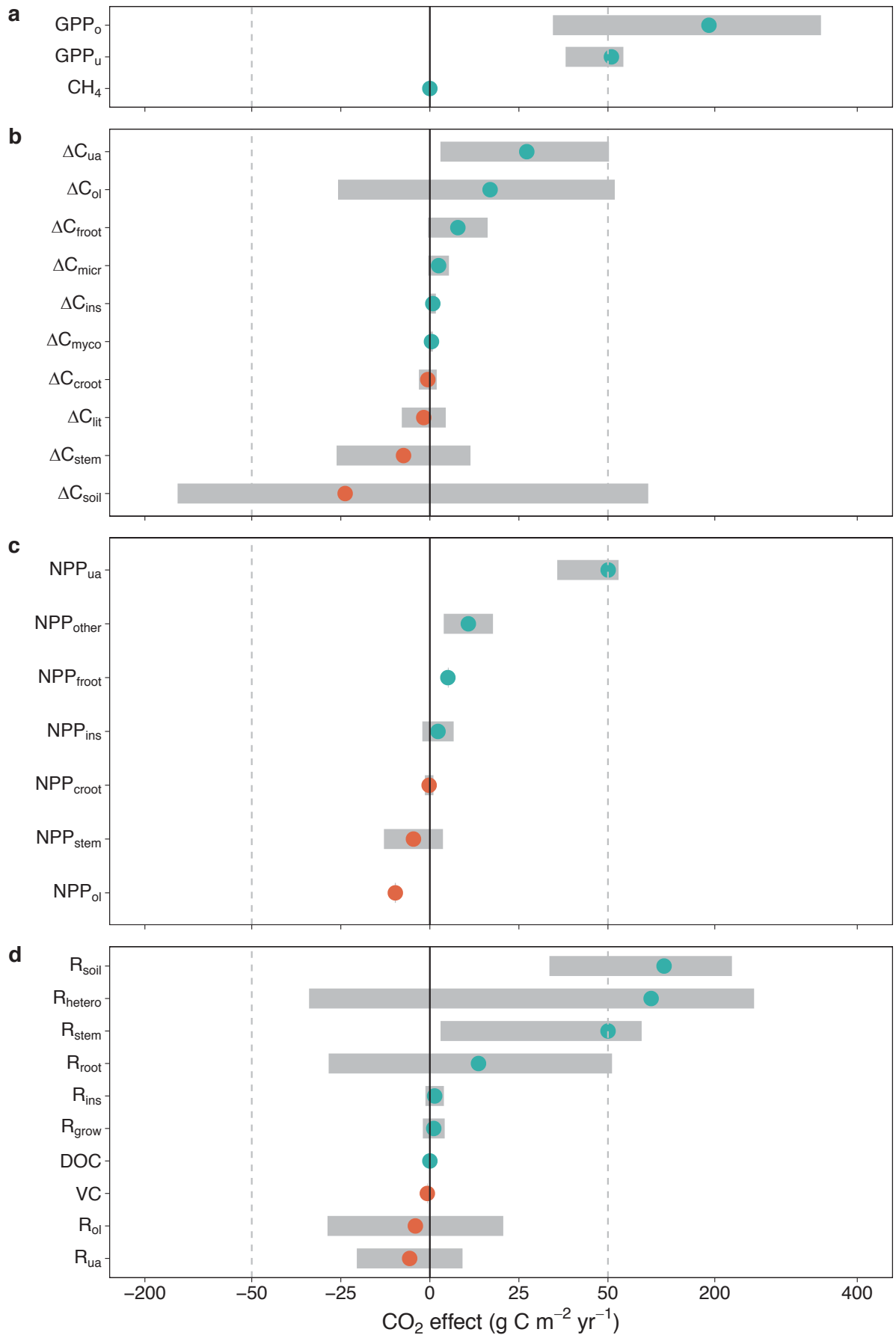
859 **Extended Data Figure 4. CO_2 treatment effect ($gCm^{-2}yr^{-1}$) for all ecosystem fluxes at**

860 **EucFACE. a)** The CO_2 response of gross ecosystem carbon uptake, including gross primary

861 production of overstorey (GPP_o) and understorey (GPP_u), and soil methane uptake (CH_4). **b)**

862 The eCO_2 response of annual incremental change in carbon pool (ΔC_{pools}), including overstorey

863 leaf (ΔC_{ol}), stem (ΔC_{stem}), coarse root (ΔC_{croot}), fineroot (ΔC_{froot}), understorey aboveground

864 (ΔC_{ua}), leaf litter (ΔC_{lit}), soil (ΔC_{soil}), microbe (ΔC_{micr}), aboveground insect (ΔC_{ins}), and

865 mycorrhizae (ΔC_{myco}). **c)** The eCO_2 response of net primary production (NPP), including

866 overstorey leaf (NPP_{ol}), stem (NPP_{stem}), coarse root (NPP_{croot}), fineroot (NPP_{froot}), understorey

867 aboveground (NPP_{ua}), twigs, barks and seeds (NPP_{other}), and leaf insect consumption (NPP_{ins}).

868 **d)** The eCO_2 response of ecosystem respiration (R) and other out-going flux, including

869 respiration fluxes of overstorey leaf (R_{ol}), stem (R_{stem}), root (R_{root}), understorey aboveground

870 (R_{ua}), growth (R_{grow}), insect (R_{ins}), heterotroph (R_{hetero}), and soil (R_{soil}), and volatile carbon

871 emission (VC) and dissolved organic carbon leaching (DOC). Dots and grey bars represent

872 means and standard deviations of the CO_2 treatment difference, predicted by a linear mixed-

873 model with plot-specific pre-treatment leaf area index as a covariate. Orange dots indicate

874 negative means and light green dots indicate positive means. Dashed lines indicate change of

875 scale along the x-axis.

876